PERFORMANCE EVALUATION OF ZERO-FORCING EQUALIZATION FOR F-OFDM SIGNALS IN THE PRESENCE OF PHASE NOISE AND FADING

A Thesis Submitted in Partial Fulfillment of Requirement for the Award of the Degree of

MASTER OF ENGINEERING

IN

ELECTRONICS AND COMMUNICATION

Submitted By:

GAGANJOT SINGH LAMBA

Roll No. 801661005

Under Supervision of

DR. AMIT KUMAR KOHLI

Associate Professor, ECED, TIET

THAPAR INSTITUTE
OF ENGINEERING & TECHNOLOGY
(Deemed to be University)

ELECTRONICS AND COMMUNICATION ENGINEERING DEPARTMENT
THAPAR INSTITUTE OF ENGINEERING & TECHNOLOGY
(A DEEMED TO BE UNIVERSITY), PATIALA, PUNJAB, INDIA

JULY, 2018

DECLARATION

I, **Gaganjot Singh Lamba**, hereby declare that the work presented in this thesis entitled **"Performance Evaluation of Zero-Forcing Equalization for F-OFDM Signals in the Presence of Phase Noise and Fading,"** in the partial fulfillment of the requirement for the award of degree of Master of Engineering (Electronics and Communication) submitted in Electronics and Communication Department, Thapar Institute of Engineering & Technology (T.I.E.T., Deemed to be University), Patiala, India is an authentic record of my own work carried out under the supervision/guidance of **Dr. Amit Kumar Kohli** (Associate Professor), Electronics and Communication Department, T.I.E.T., Patiala from 2017-2018.

The matter presented in this thesis has not been submitted either in part or full to any other university or institute for the award of any other degree.

Gaganjot Singh

Date: 12/7/2018

Gaganjot Singh Lamba
Roll No. 801661005

It is to certify that the above statement made by the candidate is correct to the best of my knowledge and belief.

Amit Kohli 12/7/2018

Date: 12/7/2018

Dr. Amit Kumar Kohli
Associate Professor, ECED,
TIET, Patiala, Punjab, India

ACKNOWLEDGEMENT

I am using this occasion to express my gratitude to my supervisor **Dr. Amit Kumar Kohli**, Associate Professor, Electronics and Communication Department (ECED), Thapar Institute of Engineering and Technology, Patiala, who supported me throughout this course work. I am thankful for his aspiring guidance, invaluably constructive criticism and fruitful advice throughout the course of the thesis research work. I am sincerely grateful to him for sharing his truthful as well as illuminating views and motivation that enhanced the improvement of my research work.

I would like to express sincere thanks to **Dr. Alpana Aggarwal**, The Head, Electronics and Communication Engineering Department (ECED), Thapar Institute of Engineering and Technology, Patiala, India for providing me with adequately friendly and professional environment for me to accomplish my work.

It was a great opportunity for learning and professional development. I will strive to utilize gained skills and knowledge in the best possible way, and will continue to work on their enhancement, in order to achieve desired career objectives.

Also, I would like to express my thanks and appreciation to all the persons, who in their own ways helped me out with the work to achieve the goals.

Gaganjot Singh Lamba

ABSTRACT

In this thesis report, we present the performance evaluation of a low-complexity fast – orthogonal–frequency–division–multiplexing (F–OFDM) scheme, in the presence of phase-noise (PHN), working under the generic linear fading channels (like two-wave-with-diffuse-power (TWDP) multipath fading and modal dispersion in multi-mode-fiber optic channel). Here, a single-tap zero-forcing (ZF) equalizer is utilized to compensate the channel-impulse-response (CIR) without sacrificing data-rate, in which the discrete-cosine-transform (DCT) operation is replaced by the discrete-Fourier-transform (DFT) operation at the receiver. The phase noise variations are modeled by utilizing the random–walk paradigm, in which PHN is dependent on the model parameters/statistics. Therefore, main focus is on the impact of PHN on the performance of single-tap ZF equalization for F–OFDM signals. Simulation results are presented to illustrate efficiency and efficacy of underlying F–OFDM system, while working under TWDP, Rician and Rayleigh multipath fading linear channels. It can be inferred from results that the PHN severely affects/deteriorates the performance of F–OFDM based communication systems in terms of high bit-error-rate (BER), when the PHN variations are large. Further, a typical case of TWDP fading (where both the specular components are in opposite phase) is also investigated under similar fading conditions in the absence as well as in the presence of PHN. Moreover, the TWDP fading model is found to be quite appropriate for analyzing/investigating the BER performance of communication systems using the binary-phase-shift-keying modulation technique.

The presented research work is not only finding applications in advanced wireless communication systems, but also appearing to be appropriate choice for optical fiber communication. Future work includes the usage of discrete-sine-transform (DST) for multicarrier communication.

Keywords - Phase noise, DCT, DFT, Fast–OFDM, TWDP fading, ZF equalizer.

TABLE OF CONTENTS

LIST OF ACRONYMS

ADC	Analog to Digital Converter
ADSL	Asymmetric Digital Subscriber Line
AWGN	Additive White Gaussian Noise
BEP	Bit Error Probability
BER	Bit Error Rate
BPSK	Binary Phase Shift Keying
BW	Bandwidth
CFO	Carrier Frequency Offset
CIR	Channel Impulse Response
CPE	Common Phase Error
CSI	Channel State Information
DAB	Digital Audio Broadcasting
DAC	Digital to Analog Converter
DCT	Discrete Cosine Transform
DFT	Discrete Fourier Transform
DMT	Discrete Multitone
DSB	Double Side Band
DST	Discrete Sine Transform
DTFT	Discrete Time Fourier Transform
DTT	Discrete Trigonometric Transforms
DV	Digital Video
DVB	Digital Video Broadcasting
ETSI	European Telecommunications Standards Institute
FDE	Frequency Domain Equalization
FFT	Fast Fourier Transform
F-OFDM	Fast Orthogonal Frequency Division Multiplexing
GI	Guard Interval
HDSL	High-Bit-Rate Digital Subscriber Line
ICI	Inter Carrier Interference
IDCT	Inverse Discrete Cosine Transform
IDFT	Inverse Discrete Fourier Transform

IF	Intermediate Frequency
IFFT	Inverse Fast Fourier Transform
ISI	Inter Symbol Interference
LAN	Local Area Network
LO	Local Oscillator
LOS	Line of Sight
LTI	Linear Time Invariant
M-ASK	M-ary Amplitude Shift Keying
MC	Multicarrier
MCM	Multicarrier Modulation
MGF	Moment Generating Function
MMF	Multimode Fiber
MMSE	Minimum Mean Square Error
OFDM	Orthogonal Frequency Division Multiplexing
ONU	Optical Network Unit
P/S	Parallel to Series
PAM	Pulse Amplitude Modulation
PAPR	Peak to Average Power Ratio
PHN	Phase Noise
QAM	Quadrature Amplitude Modulation
QPSK	Quadrature Phase Shift Keying
RF	Radio Frequency
RMS	Root Mean Square
RV	Random Variable
SMF	Single Mode Fiber
S/P	Series to Parallel
SIR	Signal to Interference Ratio
SNR	Signal to Noise Ratio
SSB	Single Side Band
TO	Timing Offset
TWDP	Two Wave with Diffuse Power
ZF	Zero Forcing
ZP	Zero Padding

LIST OF FIGURES

LIST OF TABLES

Chapter 1

INTRODUCTION BASED ON LITERATURE REVIEW

1.1. Introduction About OFDM Systems

Multicarrier communication is a widely accepted scheme in wireless as well as wireline communication applications [1]–[3]. In recent years, wireless communication applications have experienced an enormous growth, as they allow high mobility. The demand for high data-rates is also increasing rapidly day-by-day. In basic communication system, single-carrier frequency is used for modulating the data. Whole available bandwidth is occupied by each symbol. However, there are some disadvantages of wireless channels, like multipath fading, which makes them difficult to be dealt with. To overcome these multipath distortions, while maintaining the high data rates, OFDM is widely used [4]. Fig. 1.1 demonstrates the basic block level representation of an OFDM. In OFDM, the single wideband system is divided into numerous narrowband parallel subcarriers. These subcarriers overlap partially with frequency bands. High speed continuous data streams can be divided into slow speed parallel data streams. Compact spectral utilization is obtained due to the separation of subcarriers. OFDM is an appealing technique because of the appropriate handling of multipath interference at the receiver. Instead of extenuating frequency-selective fading problem as a whole, OFDM mitigates the setback by converting the whole frequency-selective faded channel into number of narrow bandwidth flat-faded channels. Flat-fading allows the receiver to combat channel tracking problem and inter symbol interference (ISI) by employing simple equalization schemes.

1.1.1. *Advantages*

Numerous wireless technologies are utilizing OFDM system, and it is also probable for future wireless communication systems because of the following advantages

- *Imperviousness to frequency selective fading*: Single-carrier system does not bear any resistance to fading. OFDM splits the entire channel into various signals that individually get affected as flat-fading sub-channels.
- *Spectrum efficiency*: OFDM utilizes close spaced overlapping sub-carriers, while maintaining their orthogonality, and hence efficiently utilizing the available spectrum [5].
- *Immunity to ISI*: As each sub-channel has low data rate, this results in high resiliency to inter-symbol-interference and inter-frame-interference.

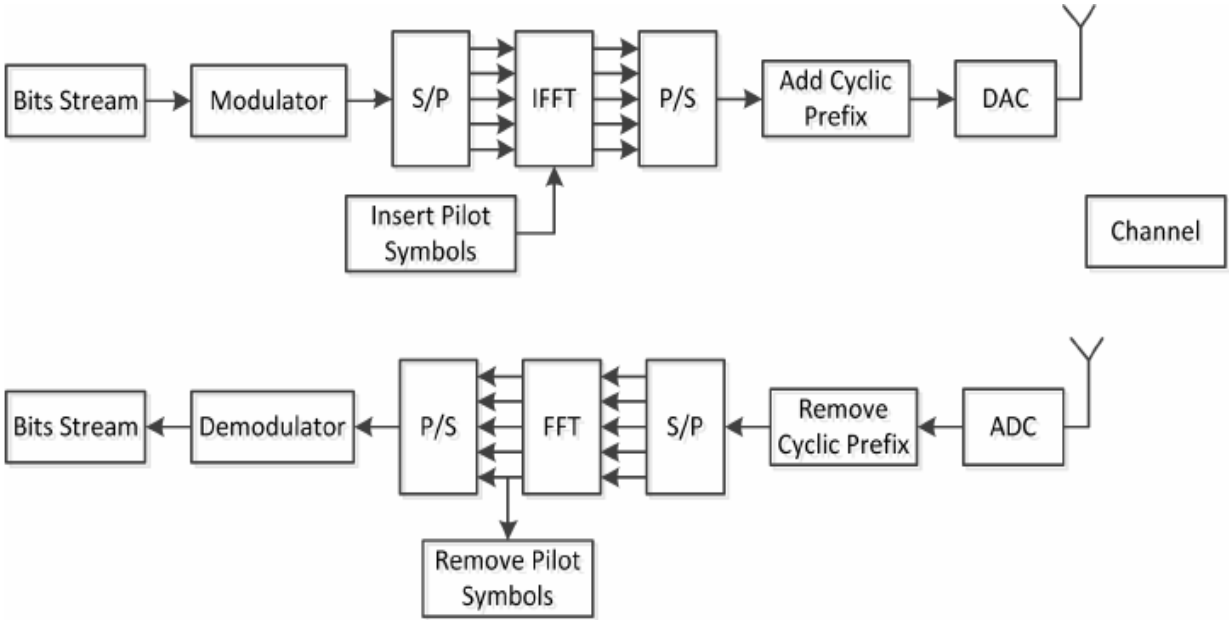

Fig. 1.1. Block level representation of OFDM communication system [6].

- *Simpler channel equalization*: Earlier, in conventional spread spectrum techniques, channel equalization has to be applied across the entire channel bandwidth resulting in an increase in channel equalization complexity. On the contrary, for OFDM, only a single-tap equalizer is required, as it uses multiple sub-channels, hence reducing equalization complexity.
- *Reduced implementation complexity*: Information transmission using OFDM can be actualized using IFFT and FFT instead of bank of modulators and demodulators, and hence making it mathematically and practically efficient [7].

1.1.2. *Disadvantages*

Even as OFDM is widely used, there are still a few drawbacks, which need to be addressed while taking into account of its use. Some of them are

- *Susceptible to carrier offset and drift*: As compared to single carrier system, orthogonal frequency division multiplexing is quite susceptible to drift as well as carrier frequency offset [8].
- *High PAPR:* OFDM signals are characterized by noise like amplitude deviation in time domain and have relatively large dynamic range leading to high PAPR [9]. As RF amplifiers need to be linear and accommodate large amplitude swings, therefore these factors make amplifiers to work on lower efficiency level.

- *Computational complexity*: Both receiver and transmitter complexity increases on increasing the number of sub-channels.

1.1.3. *Applications*

OFDM is discrete-time data transmission scheme developed into a trendy technique for wideband wireless system. The use of OFDM has increased tremendously over the last 10 years owing to its significant use in wideband high data rate transmissions. Nowadays, OFDM finds application in digital broadcasting (one to many) communication systems, like digital audio broadcasting (DAB) and digital video broadcasting (DVB).

Digital audio broadcasting is a standardized international digital broadcasting scheme, which was pioneered by European Eureka-147 Project. OFDM is now proposed for digital radio mondiale (DRM) and Eureka-147 DAB standard.

OFDM is quite useful in modem/ADSL, in which it is called discrete multitone (DMT). Here, this is utilized with phone line; hence, phone line is filtered to obtain large signal to noise ratio. High bit-rate digital subscriber line (HDSL) is also a telecommunication protocol for equal forward link and reverse link rates.

HiperLAN2 is an efficient radio system, designed by European Telecommunications Standards Institute (ETSI), which is particularly suited for operation in LAN environments. Its physical layer employs OFDM modulation. OFDM is moreover widely employed in wireless internet modems (IEEE 802.11a).

1.2. Fast-OFDM (F-OFDM)

Over the past few years, spectral efficiency in communication systems has been enhanced due to conventional OFDM system. It has been swiftly and broadly accepted in wireless, wireline and broadcast methods for efficient handling of linear signal ambiguities, arising while transmitting through dispersive faded channels. Recently, OFDM technology has found its widespread use in optical communications. This is primarily due to the advancements in discrete-time signal processing (DSP) techniques, that makes processing at very high symbol rates attainable.

Having features like high spectral efficiency and resilient behavior towards dispersion, optical orthogonal frequency division multiplexing (OOFDM) has attracted substantial attention in technical innovator community. The concept behind compatibility of OFDM modulation for communication through dispersive faded channels is that it bifurcates a high-rate information sequence into numerous low-rate information sequences, which are communicated concurrently over numerous harmonically associated narrowband subcarriers. Improved efficiency in OFDM

systems is a result of reduced subcarrier spacing. For this reason and to make an upper hand in the market, optical F-OFDM is utilized with principle focus being the reduction of transceiver components' expenses, like the analog-to-digital conversion device (ADC)/digital-to-analog conversion device (DAC). Its block level representation is shown in Fig. 1.2.

F-OFDM is a proficient multicarrier signaling scheme, with half the subcarrier spacing as that of the conventional OFDM technique [10]–[12]. In fast-OFDM system, discrete cosine transform (DCT) is opted in place of discrete Fourier transform (DFT) in order to multiplex data symbols over subchannels, moreover this technology is verified practically in test fiber-optical systems [13]–[15]. Improved tolerance towards Doppler shift as well as carrier frequency offset (CFO) in optical coherent detections are exhibited by fast-OFDM techniques, in comparison to traditional OFDM [16], [17]. Enhanced receiving equipment/system sensitivity in case of optic full-field detection is also an additional advantage of fast-OFDM system [18].

These perks make FOFDM technology an attractive multicarrier communication technique. The main problem faced by F-OFDM scheme is that (unlike DFT in conventional OFDM systems), DCTs employed in subcarrier multiplexing/demultiplexing don't exhibit any circular convolution characteristics, instead it possess symmetric convolution property as shown in [19]. The symmetric convolution requires the two data sequences to be extended symmetrically in order to make the DCT of convolution of two data sequences same as their individual DCTs product. This means that in practical implementations, single-tap equalization for fast-OFDM signal in the cosine domain is enabled, resulting in requirement of not just symmetric suffix and prefix as guard intervals, but also needs symmetric channel impulse response. Chromatic dispersion in single-mode fibers (SMF) is one example, which satisfies this condition [20]. Frequency-selective fading in any wireless communication channel and modal dispersion in multi-mode fibers (MMFs) (generic linear channels) are some examples, for which symmetrical convolution condition may not get satisfied, and therefore channel compensation by simply using single-tap equalizers is not easy.

Al-Dhahir *et al.* as well as Mandyam addressed this issue by proposing various techniques to meet the requirement of convolving sequences symmetrically [21], [22]. In [21], the need for channel symmetry is avoided by extending the F-OFDM signal symmetrically. However, this leads to reduction of data rates to half. The scheme demonstrated in [22] prevents the data rate reduction at the receiver by utilizing a typical time-domain finite impulse response (FIR) prefiltering on the basis of minimum-mean-square-error (MMSE) criterion to filter CIR to be symmetrical. Though, system computational burden is increased substantially. Frequency-

domain equalization (FDE) is a more effective technique [23], in which compensation of channel impairment is done at receiver side in frequency-domain before the transformation of signaling waveform to the cosinusoidal domain by the application of DCT. Requirement of two more DFT operation blocks is there at receiving side. Additionally, as the channel equalization (in frequency-domain) is done and information signaling waveforms detection (in cosinusoidal domain) is done, after DCT operation; the noise added in frequency-domain is observed to spread (after amplification) upon other subcarriers.

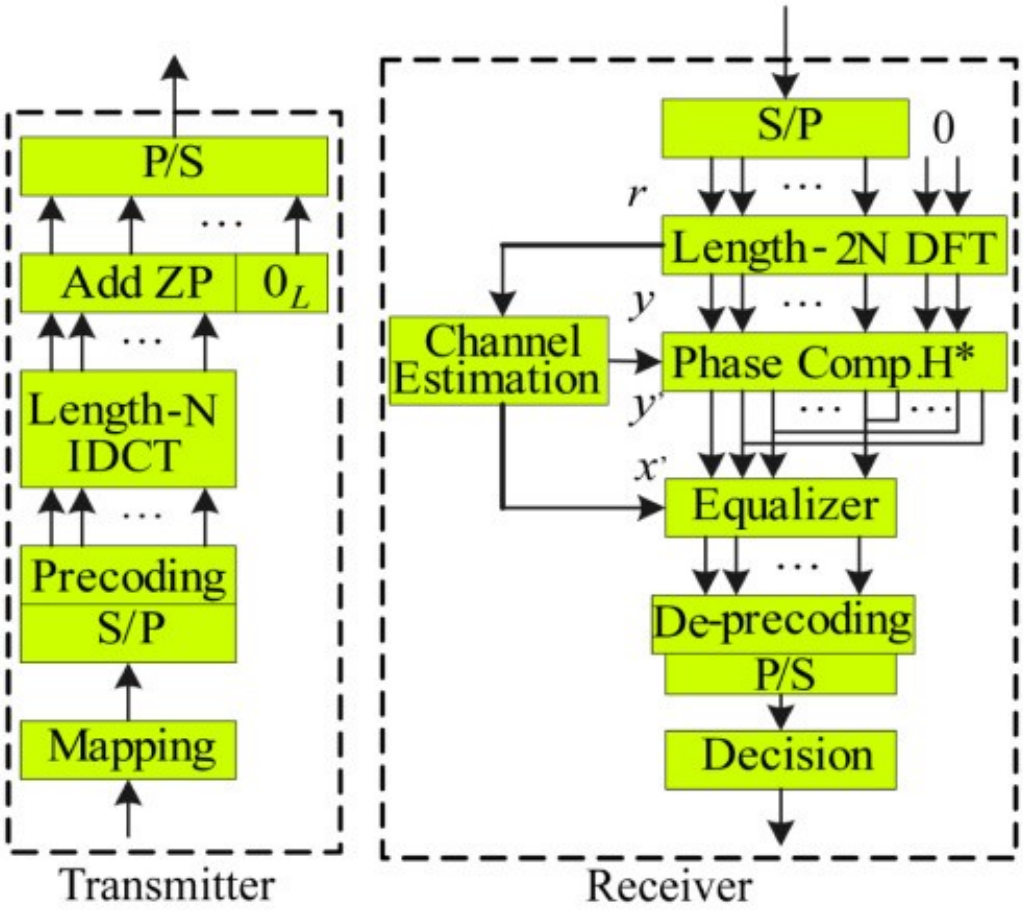

Fig. 1.2. Block level representation of F-OFDM communication system [12].

The F-OFDM technique does not sacrifice performance by using real operations, but also it reduces complexity and also its architectural design cuts down software and hardware engineering efforts. Simplicity of F-OFDM systems allows not only simplified computations, but an equivalent reduction in processing power is also a benefit. In comparison to traditional multicarrier communication technique, that utilizes real-valued fast Fourier transform (FFT) and

inverse FFT (IFFT), F-OFDM system works with half the subcarrier spacing (as depicted in Fig. 1.3) using single-dimension modulating formats considering only in-phase signal-space points.

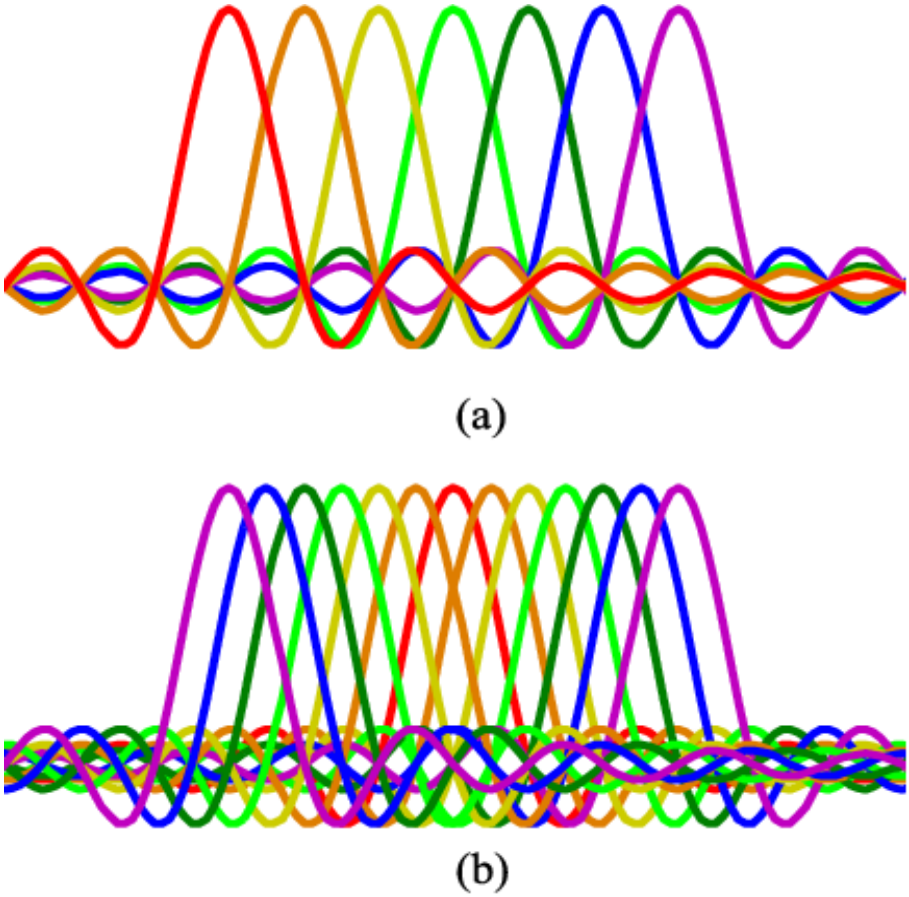

Fig. 1.3. Spectra of DFT-based OFDM and F-OFDM.
(a) DFT-based OFDM, and (b) F-OFDM [14].

Binary-phase-shift-keying (BPSK) as well as M-ary amplitude-shift-keying (M-ASK) are some typical illustrations of single-dimensional modulation formats. Amplified inter-carrier-interference (ICI) between adjacent narrowband F-OFDM subcarriers in the quadrature axis forbids the usage of two-dimensional modulating formats for example quadrature-amplitude-modulation (QAM).

Recently, effective implementation of F-OFDM technique has been done experimentally for double-side-band (DSB) signaling waveforms in systems based on single-mode-fiber utilizing the DCT. On the contrary, on considering single-side-band (SSB) signals, DFT has been favored because of high intricacy of Hilbert transformation operation, when DCT-SSB signaling techniques are used. Additionally, F-OFDM technique's study over multimode fiber links as well

as wavelength-division-multiplexing (WDM) passive optical networks (PONs) have demonstrated that this technique has great potential to attain signaling waveform transmission capacities of 3.9 Gbps over 300 m, furthermore 10 Gbps for 16 symmetric colorless fiber-optic transmission network units (ONUs) upto 25 km, respectively.

1.3. Discrete-Fourier-Transform (DFT)

In mathematics, DFT is an operation used for Fourier analysis of finite discrete-time domain signaling waveforms. This has been extensively utilized in signal processing as well as associated domains to examine the frequencies of a sampled signaling waveforms, to carry out convolution operation and to resolve complex partial differential equations. The DFT can be calculated proficiently in practice by utilizing a FFT procedure.

Because FFT procedures are so often used to evaluate DFT, these two terms are commonly employed interchangeably in real-time practices, even though there is an obvious difference, "DFT" is referred to as a mathematical operation, despite how it is calculated, whereas "FFT" is referred to as one of the numerous proficient procedures for computing DFT. This dissimilarity is further vague, however, due to the synonym "finite Fourier transform" for DFT.

1.3.1. *Definition*

The complex data information symbol stream $x_0,...,x_{N-1}$ of N length is transformed into $X_0,...,X_{N-1}$ by utilizing discrete Fourier transform, described as

$$X_q = \sum_{p=0}^{N-1} x_p e^{-\frac{j2\pi qp}{N}} \qquad q = 0,...,N-1, \tag{1.1}$$

where, e is the natural logarithm's base and $j = \sqrt{-1}$. The IDFT of corresponding sequence is according to the formula

$$x_p = \frac{1}{N}\sum_{q=0}^{N-1} X_q e^{\frac{j2\pi pq}{N}} \qquad p = 0,...,N-1. \tag{1.2}$$

Note that the normalization factor 1 and 1/N multiplying the DFT and IDFT respectively as well as the signs in the exponents are only conventions, moreover they may change in various cases. The two condition for these norms are that DFT and IDFT must be opposite in sign of their exponentials, and consequently their normalization factors should be equal to 1/N on multiplication.

To make the transform unitary, a normalization factor equal to $1/\sqrt{N}$ is used for both DFT and IDFT, as it has various theoretical advantages, however, it is frequently more handy in mathematical computations to achieve normalization all at once.

1.3.2. *Properties of DFT*

- *Completeness*

The DFT is the invertible, linear transformation operation $f : Z^N \to Z^N$; whereas, Z is a complex set of numbers, which means that a complex set of vectors will have complex vector set for DFT as well as IDFT.

- *Orthogonality*

The vectors $e^{\frac{j2\pi qp}{N}}$ are the basis for orthogonality over the *N*-dimensional complex vector set

$$\sum_{p=0}^{N-1} e^{\frac{j2\pi qp}{N}} \left(e^{-\frac{j2\pi q^1 p}{N}} \right) = N\delta_{qq^1}, \tag{1.3}$$

where, δ_{qq^1} is the Kronecker delta function. Here stipulation of orthogonality is further utilized to obtain IDFT formula from DFT's definition.

- *Periodicity*

This means that on evaluating the DFT for all integral points q in place of just $q = 0,...,N-1$ will result in an infinite sequence (periodical extension of DFT pertaining to period duration *N*). This periodicity may be illustrated as

$$X_{q+N} = \sum_{p=0}^{N-1} x_p e^{-\frac{j2\pi(q+N)p}{N}} = \sum_{p=0}^{N-1} x_p e^{-\frac{j2\pi qp}{N}} e^{-j2\pi p} = \sum_{p=0}^{N-1} x_p e^{-\frac{j2\pi qp}{N}} = X_q, \tag{1.4}$$

where, we have utilized the fact that $e^{-j2\pi} = 1$. Likewise, the IDFT formula also results in the periodical extension.

- *Circular convolution theorem and cross-correlation theorem*

The vector $x \otimes y$ is circular (cyclic) convolution of the two vectors x = x_k and y = y_k, and it can be denoted as

$$\left(x \otimes y\right)_p = \sum_{q=0}^{N-1} x_q y_{p-q} \quad p = 0,...,N-1, \tag{1.5}$$

where, y is continued cyclically so that

$$y_{-q} = y_{N-q}, \qquad q = 0,...,N-1. \tag{1.6}$$

The DFT transforms circular convolutions into element to element multiplication. So that, if

$$z_p = \left(x \otimes y\right)_p, \tag{1.7}$$

then,

$$Z_q = X_q Y_q \qquad q = 0,...,N-1, \tag{1.8}$$

where, (X, Y, Z) corresponds to the DFTs of data sequences represented by (x, y, z). Directly computing the convolution sum (shown above), would need $O\left(N^2\right)$operations, but the FFT gives an $O(N \log N)$ technique to calculate the same thing.

1.3.3. *Applications*

Most DFT applications are critically dependent on the availability of fast algorithms for computing DFTs and IDFTs.

- *Partial differential equations*

DFTs are frequently employed in solving partial differential equations, where yet again, it is utilized as a classical estimate for Fourier series (as it is recovered in the limit $N \to \infty$). The expansion of the signal in terms of complex exponentials e^{j2nx} (that is a set of eigen functions of differentiation: $\frac{d}{dx} e^{j2nx} = j2ne^{j2nx}$) is the main advantage of this approach.

Therefore, differentiation is easy in Fourier representation,—we only need to multiply with $j2n$. A linear differential equation having invariable coefficients is changed to a simply solvable algebraic equation. Now to transfer it back into the ordinary spatial representation, IDFT is used. This technique is called spectral method.

- *Spectral analysis*

When using it for the purpose of spectral analysis, the data sequence $\left\{x_p\right\}$ generally correspond to a finite set of equally-spaced time-domain samples of a random signal $x(t)$, in which t symbolizes time. This transformation to discrete-time domain from continuous-time domain alters the considered Fourier transform of $x(t)$ into discrete-time-Fourier-transform (DTFT) that normally involves a kind of inevitable error/distortion known as aliasing. Here, key to minimize this distortion is dependent on the selection of an appropriate sample-rate (Nyquist criteria). In same way, the conversion from an extremely large (or infinite) data sequence to a convenient amount involves another kind of distortion known as leakage, and that is viewed as the loss of detail (resolution) in discrete-time-Fourier-transform. Discrete sampling of DTFT (continuous frequency domain) gives the DFT (discrete frequency-domain). The inadequacy in performing

multiplications as well as summation is much greater than the offset introduced due to inherent effectiveness of FFT. As previously discussed, these distortions inflict a bound on intrinsic resolution of DTFT.

- *Data compression*

The domain of discrete time signal processing depends largely on operations in frequency-domain (pertaining to Fourier transform). For example, a number of lossy images as well as sound compression techniques incorporate DFT. Here, the signal is segregated into small segments where eachone is first transformed. Subsequently, Fourier coefficients exhibiting large frequencies (considered quite redundant) are eliminated. Furthermore, decompressor calculates the inverse transformation on the basis of alleviated number of Fourier coefficients (compression implementations usually utilize the particular type of discrete Fourier transform, which is referred to as DCT or also known as modified DCT).

- *Multiplication of large integers*

The computationally fast well known procedures for multiplications of high valued integers or polynomials are dependent on DFT operation: the information symbol streams of digits or coefficients are usually assumed to be vectors, whose convolution is required to be calculated. For conducting this operation, such frequencies are firstly Fourier transformed, and subsequently multiplied element wise. Furthermore, these are transformed back finally.

1.4. Discrete-Cosine-Transform (DCT)

A discrete cosine transform is another Fourier-related transformation operation (using only real numbers) quite similar to the DFT. DCTs are comparable with DFTs of approximately double the length, working upon real data having even symmetry (as real and even functions' Fourier transform give a real and even function), whereas in a few types either input data or the output sequence or both are displaced by half a sample.

Similar to various transforms, DCT attempts towards decorrelation of the image data. After decorrelating, all transformed coefficients can be encoded separately without the loss of compression efficiency. Like many other Fourier-related transforms, DCT transformed signal is expressed as a function or the summation of sines with diverse frequencies as well as amplitudes. Similar to the DFT, a DCT operation is limited to a sequence with the finite count of discrete information signal sample points. Here, clear differences the DCT and the DFT have are that latter utilizes both sinusoidal and cosinusoidal functions (as complex exponentials), while the former utilize only real valued cosinusoidal function. Nonetheless, this dissimilarity is just a

result of deeper distinction: a DCT operation and a DFT operation have different boundary conditions.

The finite domain functions, like the DFT or a DCT or a Fourier series, utilize Fourier-related transforms that define an expansion of these functions outside the domain. To be exact, once a function $f(x)$ is expressed into the summation of sines, we can calculate the sum for any x, even when true $f(x)$ was unspecified. A DFT operation, akin to Fourier series, involves a periodical extension of the true function, while the DCT uses an even extension of that function.

As DCT operates on finite and discrete sequences, two concerns come up unlike that in the continuous cosine transform. Firstly, function must be specified to know that whether it is odd or even at the boundaries (both right as well as left) of the domain. Secondly, the point has to be specified around which, the function is odd or even. Particularly, assume a data sample stream a, b, c, d with four uniformly-spaced sample points with a specified even left boundary. It exhibits two reasonable alternatives that data might be even about a sample point a. Under this scenario, even extension is dcb, a, bcd; or this sequence can be even about the point halfway (amid a and preceding point), and in this case, even extension is dcb, aa, bcd (repetition of a is there).

1.4.1. *Types and Their Definition* [24]

- $DCT-I$

The DCT-I is an exact equivalent (overall scale factor of 2) of the discrete Fourier transform of $2N-2$ real data inputs having an even symmetry. For instance, a DCT-I of $N=5$ real numbers $abcde$ is equal to half of the discrete Fourier transform of $N=8$ real numbers $abcdedcb$ having even symmetry. (On the contrary, DCT from type II to type IV involves a half-sample shift in the corresponding DFT)

$$\left(\mathrm{C}_{1\mathrm{e}}\right)_{k,j} = 2a_j \cos\left(\frac{kj\pi}{N}\right),\ 0 \le k, j \le N, a_0 = 1/2 = a_N, a_j = 1,\ j \ne 0, N, \qquad \text{(even DCT)} \qquad (1.9)$$

$$\left(\mathrm{C}_{1\mathrm{o}}\right)_{k,j} = 2a_j \cos\left(\frac{2kj\pi}{2N-1}\right),\ 0 \le k, j \le N-1, a_0 = 1/2, a_j = 1,\ j \ne 0. \qquad \text{(odd DCT)} \qquad (1.10)$$

DCT-I only works when $N \ge 2$. However, rest discrete cosine transform types are determined for every +ve N.

- $DCT-II$

Most commonly used discrete cosine transform form is DCT type II, and this is usually referred to as "the DCT". This type II transform is an exact equivalent (overall scale factor of 2) of a

discrete Fourier transform of $4N$ real numbers having even symmetry with zero valued even-indexed coefficients.

$$\left(\mathrm{C}_{2\mathrm{e}}\right)_{k,j} = 2\cos\left(\frac{k(2j+1)\pi}{2N}\right),\ 0 \le k, j \le N-1, \qquad \text{(even DCT)} \quad (1.11)$$

$$\left(\mathrm{C}_{2\mathrm{o}}\right)_{k,j} = 2b_k \cos\left(\frac{k(2j+1)\pi}{2N-1}\right),\ 0 \le k, j \le N-1\ b_k = 1, k \ne N-1, b_{N-1} = 1/2\,. \quad \text{(odd DCT)} \quad (1.12)$$

DCT-II matrix is an orthogonal matrix, but for half-shifted input, its direct relation with a real-even DFT is broken.

- $DCT-III$

This is also an inverse of DCT-II, as a result DCT type III is often referred to as "the inverse DCT" ("IDCT").

$$\left(\mathrm{C}_{3\mathrm{e}}\right)_{k,j} = 2a_j \cos\left(\frac{(2k+1)j\pi}{2N}\right),\ 0 \le k, j \le N-1, a_0 = 1/2, a_j = 1, j \ne 0\,, \qquad \text{(even DCT)} \quad (1.13)$$

$$\left(\mathrm{C}_{3\mathrm{o}}\right)_{k,j} = 2a_j \cos\left(\frac{(2k+1)j\pi}{2N-1}\right),\ 0 \le k, j \le N-1, a_0 = 1/2, a_j = 1, j \ne 0\,. \qquad \text{(odd DCT)} \quad (1.14)$$

The DCT types II and III are also transposes of each other. As a result of which, DCT-III matrix is also an orthogonal matrix, but it also hampers direct relation with the real-even discrete Fourier transform of half-shifted output.

- $DCT-IV$

$$\left(\mathrm{C}_{4\mathrm{e}}\right)_{k,j} = 2\cos\left(\frac{(2k+1)(2j+1)\pi}{4N}\right),\ 0 \le k, j \le N-1, \qquad \text{(even DCT)} \quad (1.15)$$

$$\left(\mathrm{C}_{4\mathrm{o}}\right)_{k,j} = 2\cos\left(\frac{(2k+1)(2j+1)\pi}{4N+2}\right),\ 0 \le k, j \le N-1\,. \qquad \text{(odd DCT)} \quad (1.16)$$

The DCT-IV matrix can be converted into orthogonal matrix, thus also evidently symmetric and its own inverse, when it is multiplied by $\sqrt{2/N}$ scaling factor.

1.4.2. *Inverse DCT* [25]

Utilizing the above conventions for normalization, the inverse of DCT-I is multiplication of DCT-I by the factor $2/(N-1)$. The inverse of DCT-IV is multiplication of DCT-IV by a factor 2/*N*. The inverse of DCT-II is multiplication of DCT-III by a factor 2/*N* and vice versa.

Similar to DFT, normalization factor used in the definitions of aforementioned transforms is solely a tradition and further differentiates between these operations. However, a number of authors multiply these transforms by a factor of $\sqrt{2/N}$, so that no additional multiplicative factor is required for their inverse.

1.4.3. *Properties of DCT*

- *Decorrelation*

Main benefit of image transformation is that undesired redundancy is removed in between adjacent pixels. It results in uncorrelated transformation elements that may be encoded in an independent manner. After the DCT operation, the autocorrelation amplitude is quite small at each interval. Therefore, it can be deduced that outstanding decorrelation properties are exhibited by DCT.

- *Energy Compaction*

Effectiveness of a transformation technique lies in its capability of packing an input sequence into a minimum possible number of coefficients. This permits the quantizer to remove coefficients having comparatively small amplitudes with no introduction of visual alteration in the reconstructed image.

- *Orthogonality*

Orthogonality is maintained by DCT basis functions. Therefore, its inverse transform matrix M has been found equivalent to its transpose i.e., $M^{-1} = M^{T}$. Thus, besides its decorrelation characteristics, some reduction in the pre-computation complexity is also provided by this property.

1.4.4. *Applications*

The discrete cosine transform, is usually exploited in image as well as signal processing, particularly in case of lossy data compression, since DCT exhibits a robust "energy compaction" feature[19]. The majority of signal information is likely to be concerted on little number of lower frequency coefficients of discrete cosine transform, approximating Karhunen-Loève transformation (most favorable in decorrelation terms) for signaling waveforms depending on typical limiting conditions for Markov processes.

For instance, utilization of DCT lies in JPEG image compression, DV, MPEG, as well as in MJPEG video compression [25]. Here, the computation of 2-dimensional discrete cosine transform of $N \times N$ blocks is done, then its outcome is quantized along with entropy coded. For such illustration, the DCT-II formula, with N=8, is carried out on all rows as well as columns of underlying block. Its outcome is the 8 × 8 transformation coeff.s' array with (0,0) element being a DC (0-frequency) constituent, and the other components with increase in horizontal as well as vertical indices symbolize the higher horizontal and vertical spatial frequencies. A similar transform (DCT-IV based), the modified-DCT (MDCT), has been utilized for MP3, vorbis as well as AAC audio compression.

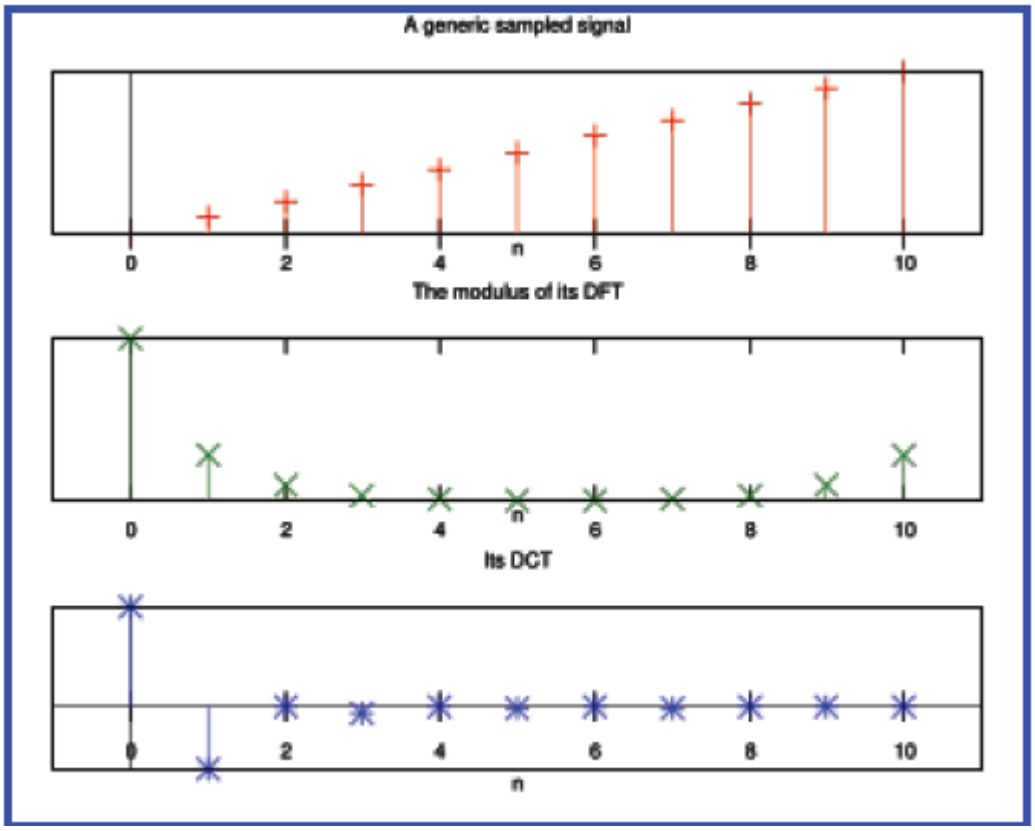

Fig. 1.4. Input signal (top), its DFT (middle), and its DCT (bottom) [16].

DCTs are further extensively utilized in resolving partial differential equations using spectral techniques, where somewhat varying odd/even boundary conditions at two extremes of array corresponds to some different variants of the DCT.

DCTs are strongly associated with Chebyshev polynomials. However, fast discrete cosine transform schemes have also been employed for Chebyshev approx. of random functions using a sequence of Chebyshev polynomials, for instance in Clenshaw-Curtis quadrature.

1.5. Types of Fading Scenarios

Fading is rapid fluctuation in signal strength caused because of destructive mixing of two or more versions of transmitted signaling waveform. It is the main bottleneck in designing wireless communication models.

1.5.1. *Conventional Fading Scenario*

Rayleigh and Rician fading models are conventionally used models to properly characterize any fading environment. Hence, these two models are presented before discussing TWDP fading model.

1.5.2. *Rayleigh Fading Scenario* [26]

Rayleigh fading scenario consists of many diffuse components with no strong LOS component. It is often considered as worst case fading scenario, and thus many practical wireless systems are designed considering this fading scenario. Also mobile radio channels are often considered to exhibit the Rayleigh distribution to illustrate the statistical time varying nature of received signal.

It has multipath components each with random phase and amplitude. Its pdf is defined as

$$f_R(r) = \frac{r}{\sigma^2} \exp\left(\frac{-r^2}{2\sigma^2}\right), \quad r \geq 0, \tag{1.17}$$

where, r represents the fading amplitude, σ denotes the RMS strength of voltage signal received, and σ^2 denotes of received signal's average power before envelope detection.

This fading environment is modeled using two random variables, such that

$$V_r = X + jY, \tag{1.18}$$

where, X and Y are two RVs having zero mean and σ^2 variance, and thus, the fading amplitude at ith time is given by

$$r_i = \sqrt{x_i^2 + y_i^2}. \tag{1.19}$$

1.5.3. *Rician Fading Scenario* [26]

Rician fading scenario consists of one strong LOS component along with many diffuse components. In such case, diffuse components coming at variable angles are superimposed with that of stationary specular i.e., dominant component. Its pdf is defined as

$$f_R(r) = \frac{r}{\sigma^2} \exp\left(\frac{-r^2 - V_1^2}{2\sigma^2}\right) I_0\left(\frac{rV_1}{\sigma^2}\right), \qquad r \geq 0, \tag{1.20}$$

where, r denotes the fading amplitude, parameter V_1 represents the maximum amplitude of specular constituent; whereas I_0 indicates modified Bessel function of zero-order and first kind.

Fading amplitude r_i at ith time instant is given by

$$r_i = \sqrt{(x_i + V_i)^2 + y_i^2}, \tag{1.21}$$

where, V_i is amplitude of specular constituent; x_i and y_i are random variables having zero mean and σ^2 variance. Rician distribution is commonly analyzed using value of parameter K_{Ric}, which denotes ratio of power of specular component to that of the diffuse component, which is given by

$$K_{Ric} = \frac{V_i^2}{2\sigma^2}, \tag{1.22}$$

1.5.4. *Two Wave With Diffuse Power (TWDP)* [26] *Fading Scenario*

Two wave with diffuse power fading includes two strong LOS components along with many diffuse components. This model has attracted attention, since current wireless scenarios are correctly characterized by this fading model. Efficient wireless communication requires that transmitter and receiver are well designed, which requires knowledge of fading environment. Hence, it is imperative to analyze and design this fading type, so that any wireless scenario suiting particular environment may be appropriately/approximately represented. It has two parameters, which are K and Δ.

$$K = \frac{V_1^2 + V_2^2}{2\sigma^2}, \ \Delta = \frac{2V_1V_2}{V_1^2 + V_2^2}, \tag{1.23}$$

where, V_1 and V_2 are magnitudes of voltages of two specular waves, while $2\sigma^2$ denotes mean power of diffuse waves. K represents ratio of specular power to that of the diffuse power, whereas Δ is relative strength of its specular constituents.

TABLE 1.1 CATEGORIZATION OF FADING ON THE BASIS OF NUMBER OF SPECULAR COMPONENTS.

TYPE OF FADING	NUMBER OF SPECULAR COMPONENTS
Rayleigh fading	No specular component
Rician fading	One specular component
TWDP fading	Two specular components

Table 1.1 classifies fading on the basis of number of specular components. Rayleigh has zero LOS path, while there is one strong LOS component in Rician fading and two strong LOS components in TWDP fading.

1.6. Problem Statement

The IDCT/DCT based communication systems are compatible with wireless as well as wireline data transmission scenarios. However, like IDFT/DFT based communication systems, the IDCT/DCT based communication systems also suffer as a result of PAPR, frequency offset, and

phase noise. Therefore for fast-OFDM information data transmission systems, discrete cosine transform based approach appears to be an appropriate choice while operating under the TWDP fading channels, when phase noise is found to be inevitable.

In the presented research work using IDCT/DFT based communication systems, we mainly address the effect of phase noise on single-tap zero-forcing equalization for F-OFDM signals under generic linear faded channels. The utility of TWDP fading channel model is also discussed, when BPSK modulation technique is employed in the underlying communication system.

Chapter 2

IDCT/DCT BASED COMMUNICATION SYSTEMS WORKING UNDER FADING CHANNELS

2.1. Introduction

Besides finding application at physical layer of numerous wireless networking standards, like HIPERLAN/2, IEEE 802.11a as well as IEEE 802.16a, multicarrier modulation (MCM) is utilized in wireline digital communication systems as well, for instance ADSL. These are DFT-based MCM systems, in which the sets of complex exponent functions are utilized as the orthogonal basis.

In spite of the efficiency in fighting against multipath fading channels, DFT-based systems suffer from certain drawbacks, like the sensitivity towards carrier frequency offsets (CFOs), or large peak-to-average power ratio. For mobile OFDM transmissions, interferences caused by the frequency offset mainly occur due to the movement-induced Doppler shift and the difference or non-stability in local oscillators of transmitter/receiver. It is quite well-known that bit error probability (BEP) is directly affected by the Doppler spectrum broadening occurring due to the speed of the terminal. For correction of CFO and other downsides, different solutions employ DTTs, primarily DCT Type-II (even) in multicarrier modulation [16], [21], [22], [27]. Energy compaction of DCT leads to the smaller amount of inter-carrier interference leakage to neighboring subcarriers in DCT-MCM as compared to DFT-MCM, resulting in the enhanced output characteristics with sturdiness to frequency offset [16], [22]. Furthermore, the anti-symmetric property in DCT-MCM helps to estimate entire range of frequency offset, which gives more accurate and better robust estimation [27].

DCT-based multicarrier transceivers can be designed for both the transmitter as well as the receiver. It can be achieved by two different ways. The first way involves obtaining the constraints to utilize all types of DCTs for multicarrier information symbol communication by employing matrices. Assume a system given in Fig. 2.1, it uses both left prefix as well as right suffix, so as to introduce redundancy in the transmitted signal. The introduction of these prefix and suffix is with the objective to attain the channel matrix, which is accurately diagonalizable by discrete cosine transforms. By utilizing diagonalization features of discrete cosine transforms [28], the frequency-domain equalization configuration at the receiving end can be reduced to the

simpler configuration. Here, aforementioned matrix formulation can be used to derive the constraints for employing the DCT Type-II (even) as well as DCT Type-III (even as well as odd) pertaining to MCM.

Other means to formulate DCT-based multicarrier communication is based on interpreting symmetrical convolution. In other words, in the system described in Fig. 2.1, if discrete cosine transforms are employed like in block transformations, then idea involves forcing a linear convolution carried out via a channel to turn into the symmetrical convolution in time-domain, or equally, a point-by-point operation in equivalent discrete cosine transform domain. Due to convolution-multiplication property [19] of DCTs, the symmetrical convolution in time-domain gives similar result as that attained by using the IDCT of element-wise multiplication of forward discrete cosine transforms of those two data sample signal sets.

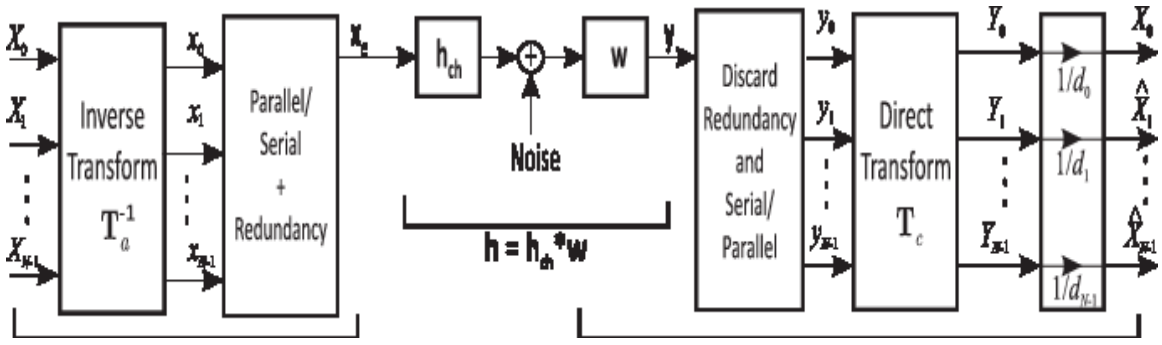

Fig. 2.1. Block level representation of a transform-based multicarrier system over an AWGN channel [24].

So, by using the convolution-multiplication property of DCTs, equalization of the effects of transmission channel with the help of one-tap per subcarrier equalizer can be done efficiently.

2.2. System Model

The OFDM systems based on DFT use complex exponential function set

$$\sqrt{\frac{1}{T}}e^{j2\pi nF_{\Delta}t}, \quad 0 \le t < T, \qquad n = 0,1,...,N-1. \tag{2.1}$$

Here, j (an imaginary unit) is the orthogonal basis. In order to sustain the orthogonality of such functions [16]

$$\int_0^T \sqrt{\frac{1}{T}} e^{j2\pi nF_\Delta t} \sqrt{\frac{1}{T}} e^{-j2\pi mF_\Delta t} dt = \begin{cases} 1, & n = m \\ 0, & n \neq m \end{cases}, \tag{2.2}$$

the minimum subcarrier spacing F_Δ required is $1/T$ Hz, where, T is the duration of the OFDM symbol excluding guard interval. Contrary to the traditional DFT-OFDM, only one set of cosine functions $\cos(2\pi nF_\Delta t)$, $n = 0,...,N-1$, is employed as the orthogonal basis for MCM implementation in DCT-OFDM. The minimum F_Δ requisite to satisfy

$$\int_0^T \sqrt{\frac{2}{T}} \cos(2\pi kF_\Delta t) \sqrt{\frac{2}{T}} \cos(2\pi mF_\Delta t) dt = \begin{cases} 1, & k = m \\ 0, & k \neq m \end{cases}, \tag{2.3}$$

is $1/T$ Hz. For baseband DCT-OFDM block, $x(t)$ may be expressed in continuous-time as

$$x(t) = \sqrt{\frac{2}{N}} \sum_{n=0}^{N-1} d_n \beta_n \cos\left(\frac{n\pi t}{T}\right), \tag{2.4}$$

here, $d_0, d_1, ..., d_{N-1}$ are N independent information symbols attained from the constellation of modulation, such that

$$\beta_n = \begin{cases} 1/\sqrt{2}, & n = 0 \\ 1, & n = 1,2,..., N-1 \end{cases}. \tag{2.5}$$

ISI is not considered, as it can be eliminated by adding an appropriate guard interval. An estimated Welch spectrum related to a 64-subcarrier DFT-OFDM as well as DCT-OFDM baseband signaling waveforms, both utilizing QPSK modulation is shown in Fig. 2.2. In spite of $1/2T$ subcarrier frequency spacing for DCT-OFDM, BW required for both DCT-OFDM as well as DFT-OFDM systems with equal number of subcarriers is equal. This is so because in order to transmit a passband DCT-OFDM signaling waveforms, there is a requirement of double transmission BW of similar lowpass signal. In this figure, the normalization of the frequency axis is done w.r.t. $1/T$ Hz. The channel bandwidth requirement for bandpass signaling waveforms of each system is equal, i.e., $64/T$ Hz. It should be noted that the baseband DCT-OFDM signal $x(t)$ is real in nature, even if information symbols d_n have been attained through real-valued modulation formats, like BPSK and PAM. Thus, single-sideband (SSB) communication scheme may be exploited to enhance BW efficiency. Therefore, in such case of real-valued modulation having equal number of subcarriers, the bandwidth required by a DCT-OFDM strategy is typically 1/2 to that of required by a DFT-OFDM system. On the other hand, SSB communication scheme cannot be employed in case of $x(t)$ being a complex-valued signal.

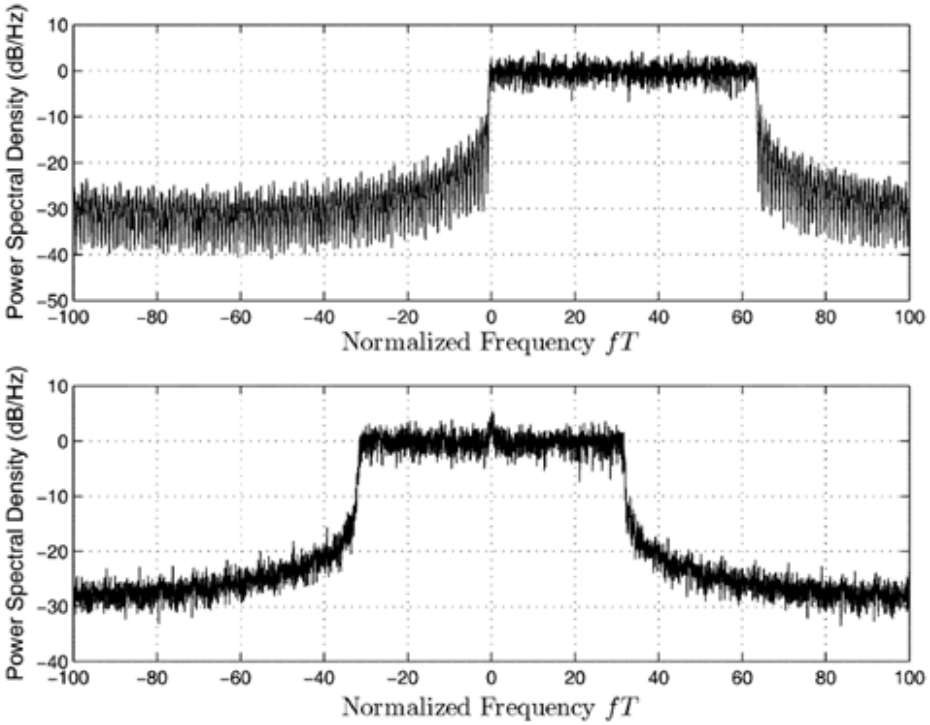

Fig. 2.2. The power spectral density of a 64-subcarrier
(a) DFT-OFDM baseband signal and
(b) DCT-OFDM baseband signal [16].

After being sampled at time intervals $t_m = T(2m+1)/2N$, the continuous-time signaling waveforms $x(t)$ provides a discrete time signal

$$x_m = \sqrt{\frac{2}{N}} \sum_{n=0}^{N-1} d_n \beta_n \cos\left(\frac{\pi n(2m+1)}{2N}\right), \quad m = 0,1,...,N-1, \tag{2.6}$$

which is the inverse DCT. Thus, $x(t)$ can be achieved by firstly applying IDCT on the input information symbol sequence

$$d = [d_0, d_1, ..., d_{N-1}]^T, \tag{2.7}$$

where, $[\ ]^T$ is the transpose operation, and then passing resulting signal sample stream $x = [x_0, x_1, ..., x_{N-1}]^T$ serially through a DAC. By ignoring noise temporarily as well as assuming the ideal channel scenario, true information symbol d_n may be obtained at receiver side, by sampling received signal as well as by implementing the discrete cosine transform, i.e.,

$$d_n = \sqrt{\frac{2}{N}} \beta_n \sum_{m=0}^{N-1} x_m \cos\left(\frac{\pi n(2m+1)}{2N}\right). \tag{2.8}$$

2.3. ICI Analysis

A detailed representation of discrete cosine transform based OFDM system with IQ modulators affected by phase error and CFO Δf is shown in Fig. 2.3. It is analogous to the discrete Fourier transform based OFDM system, as IDCT as well as DCT sections can be replaced by IFFT as well as FFT sections respectively. As discrete cosine transform is the real transformation, therefore this is unimportant to utilize quadrature modulator, if 1-D signalling format procedure is employed in a DCT-OFDM system. However, in case of DFT-OFDM, it is necessary to take account of both in-phase as well as quadrature modulator even for 1-D signalling formats, as the DFT yields complex data sets, even for the real signal.

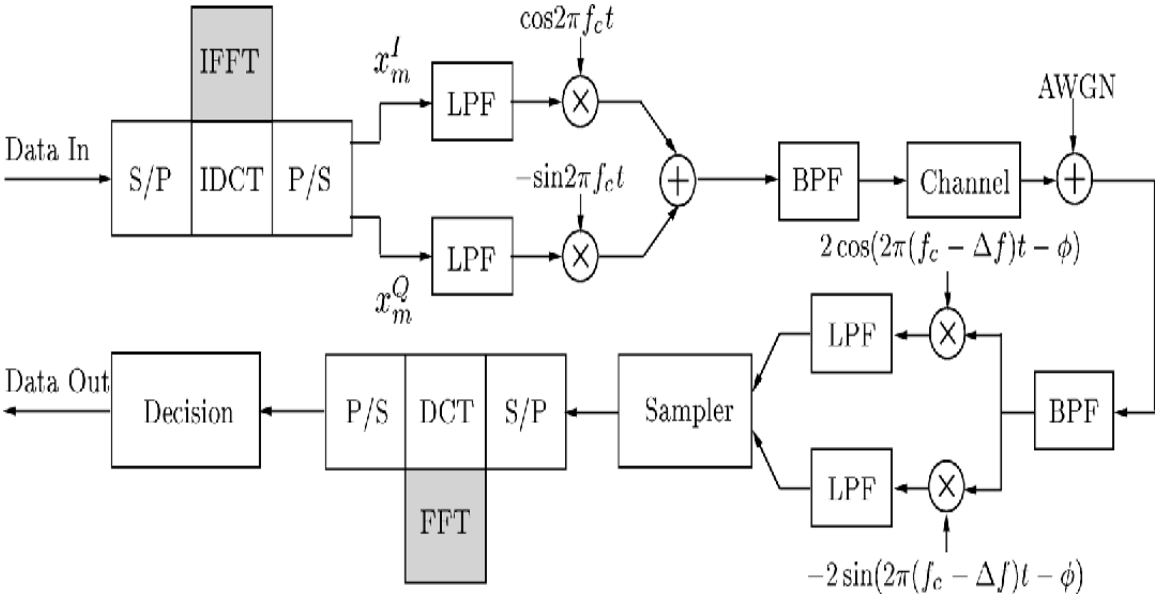

Fig. 2.3. DCT-based as well as DFT-based orthogonal frequency division multiplexing systems [16].

A sequence having in-phase components x_m^I along with quadrature-phase components x_m^Q is acquired after performing the IDCT in Fig. 2.3, as

$$x_m^I + jx_m^Q = \sqrt{\frac{2}{N}} \sum_{n=0}^{N-1} (d_n^I + jd_n^Q)\beta_n \cos\left(\frac{\pi n(2m+1)}{2N}\right), \tag{2.9}$$

where, d_n^I and d_m^Q are attained from modulation techniques, like BPSK, QPSK, and QAM. Then x_m^I and x_m^Q components are passed to the in-phase and the quadrature-phase modulators serially, respectively. Therefore, real part $x_b^I(t)$ as well as imaginary part $x_b^Q(t)$ of a baseband DCT-OFDM signal frame can be written as

$$x_b^I(t) = \sum_{m=0}^{N-1} x_m^I f\left(t - \frac{(2m+1)T}{2N}\right), \tag{2.10a}$$

$$x_b^Q(t) = \sum_{m=0}^{N-1} x_m^Q f\left(t - \frac{(2m+1)T}{2N}\right), \tag{2.10b}$$

respectively, where $f(t)$ represents the low-pass reconstruction filtering configurations, which carries out D/A conversion. As a result, a block of transmitted bandpass signalling waveforms may be defined as

$$x(t) = \Re\left\{\left[x_b^I(t) + jx_b^Q(t)\right]e^{j2\pi f_c t}\right\}, \tag{2.11}$$

where, $\Re\{\gamma\}$ represents the real part of γ. The received in-phase signalling waveforms $r^I(t)$ and quadrature signalling waveforms $r^Q(t)$, when both phase error ϕ and CFO Δf are present after demodulation in an AWGN channel, are represented as

$$r^I(t) = \sum_{m=0}^{N-1}\left[x_m^I q\left(t - \frac{(2m+1)T}{2N}\right)\cos(2\pi\Delta ft + \phi) - x_m^Q q\left(t - \frac{(2m+1)T}{2N}\right)\sin(2\pi\Delta ft + \phi)\right] + w_i(t), \tag{2.12a}$$

and

$$r^Q(t) = \sum_{m=0}^{N-1}\left[x_m^I q\left(t - \frac{(2m+1)T}{2N}\right)\sin(2\pi\Delta ft + \phi) + x_m^Q q\left(t - \frac{(2m+1)T}{2N}\right)\cos(2\pi\Delta ft + \phi)\right] + w_q(t), \tag{2.12b}$$

respectively. Where, $w_i(t)$ as well as $w_q(t)$ are each Gaussian noise having zero-average & $\sigma^2 = N_0/2$ variance, and $q(t)$ denotes cascade of transmitter and receiver filtering configurations, which satisfies the Nyquist criterion i.e.,

$$q\left(\frac{nT}{N}\right) = \begin{cases} 1, & n = 0 \\ 0, & otherwise. \end{cases} \tag{2.13}$$

The discrete samples r_k^I and r_k^Q are attained with sampling at $(2k+1)T/2N$ time instants, where $k = 0,1,...,N-1$. By expressing these samples in a complex notation, we have

$$\begin{aligned} \tilde{r}_k &= r_k^I + jr_k^Q + w_k^I + jw_k^Q, \\ &= (x_k^I + jx_k^Q)e^{j\left(\frac{2\pi\Delta fT(2k+1)}{2N} + \phi\right)} + \tilde{w}_k, \end{aligned} \tag{2.14}$$

where, $\widetilde{w}_k = w_k^I + jw_k^Q$ is considered to be complex Gaussian RVs. Here, discrete cosine transform operation yields decision variable $\hat{d}_k$ for signalling over kth subchannel at receiving side, such that

$$\hat{d}_k = \hat{d}_k^I + j\hat{d}_k^Q,$$

$$= (d_k^I + jd_k^Q)(S_{k,k}^I + jS_{k,k}^Q) + \sum_{\substack{n=0 \\ n\neq k}}^{N-1} (d_n^I + jd_n^Q)(S_{n,k}^I + jS_{n,k}^Q) + \widetilde{w}_k, \tag{2.15a}$$

where,

$$S_{n,k}^I = \frac{1}{2N}\beta_k\beta_n[\Psi(n+k-\varepsilon) + \Psi(n-k-\varepsilon) + \Phi(n+k+\varepsilon) + \Phi(n-k+\varepsilon)], \tag{2.15b}$$

$$S_{n,k}^Q = \frac{1}{2N}\beta_k\beta_n[\Gamma(n+k-\varepsilon) + \Gamma(n-k-\varepsilon) + \Lambda(n+k+\varepsilon) + \Lambda(n-k+\varepsilon)], \tag{2.15c}$$

$$\Psi(x) = \frac{\sin\left(\frac{\pi x}{2}\right)\cos\left(\phi - \frac{\pi x}{2}\right)}{\sin\left(\frac{\pi x}{2N}\right)}, \tag{2.15d}$$

$$\Phi(x) = \frac{\sin\left(\frac{\pi x}{2}\right)\cos\left(\phi + \frac{\pi x}{2}\right)}{\sin\left(\frac{\pi x}{2N}\right)}, \tag{2.15e}$$

$$\Gamma(x) = \frac{\sin\left(\frac{\pi x}{2}\right)\sin\left(\phi - \frac{\pi x}{2}\right)}{\sin\left(\frac{\pi x}{2N}\right)}, \tag{2.15f}$$

$$\Lambda(x) = \frac{\sin\left(\frac{\pi x}{2}\right)\sin\left(\phi + \frac{\pi x}{2}\right)}{\sin\left(\frac{\pi x}{2N}\right)}, \tag{2.15g}$$

$$\Psi(0) = \Phi(0) = N\cos\phi, \tag{2.15h}$$

$$\Gamma(0) = \Lambda(0) = N\sin\phi, \tag{2.15i}$$

and $\varepsilon = 2T\Delta f$. The subcarrier frequency spacing in DCT-OFDM system is found to be $1/2T$ Hz; and ε represents normalized frequency offset as related to subcarrier frequency spacing.

For normalized CFO case, $\varepsilon = 0$ in Eq.(2.15), one has

$$S_{n,k}^I = S_{n,k}^Q = 0, \quad n \neq k, \tag{2.18}$$

$$S_{k,k}^{I} = \cos\phi, \quad S_{k,k}^{Q} = \sin\phi . \tag{2.17}$$

Therefore, the decision variable $\hat{d}_k$ may be expressed in terms of

$$\hat{d}_k = \left(d_k^I + jd_k^Q\right)e^{j\phi} + \tilde{w}_k . \tag{2.18}$$

With only the fixed phase error ϕ, a decision variable can be considered as the phase-rotated equivalent of transmitted signalling waveforms, with no ICI. Hence, both DCT-OFDM as well as DFT-OFDM systems give the similar bit error rate performance in presence of phase error only.

2.4. Imperfection Analysis [29]

In earlier DCT-MCM systems, performance was analyzed with perfect transceivers with adequate guard sequence. However, practically, because of the inaccurate synchronization errors and hardware impairments, a certain amount of CFO and timing offset (TO) are ought to be present at the transceivers. Further, adequate length of prefix and suffix is not always certain for improving the bandwidth efficiency of the system.

2.4.1. *System Paradigm in Presence of Imperfections*

In *N* subcarrier DCT-MCM systems, the baseband modulated discrete-time signal x_m is written as

$$x_m = \sum_{k=0}^{N-1} a_k \beta_k \cos\left[\frac{\pi k(2m+1)}{2N}\right], \qquad m = 0,1,...,N-1, \tag{2.19}$$

where, a_k is ASK modulated information symbol being transmitted over *k*th subchannel, while parameter coefficient β_k can be expressed as

$$\beta_k = \begin{cases} \sqrt{\dfrac{1}{N}}, & k = 0 \\ \sqrt{\dfrac{2}{N}}, & k = 1,2,...,N-1 \end{cases} . \tag{2.20}$$

Taking into consideration, inter-block interference that is introduced because of system imperfection, the consequent discrete-time series can be extended from one block case to successive ones, as a result, *m*th sample in *i*th transmission block can be represented as

$$x_i(m) = \sum_{n=0}^{N-1} a_{i,n} \beta_n \cos\left[\frac{\pi n(2m+1)}{2N}\right], \qquad m = -v,...,N,...,N+v-1. \tag{2.21}$$

The receiver selects *N* consecutive beneficial data samples in the middle from each block of transmitted *N*+2*v* time-domain sampled data carried over underlying channel for further

processing and rejects the remaining 2v guard interval sampled data evenly present in front-end side. Considering the presence of sampling time offset Δk leading to the frame synchronization error, the indices of residual N samples of jth block at receiving end are $\{k-\Delta k+j(N+2v)\,|\,k=0,...,N-1\}$. In this scenario, rest of the samples $r(k)$ corresponding to jth block at receiving end following to the removal of guard symbols and channel convolution can be represented as

$$r(k)=\sum_{i=-\infty}^{+\infty}\sum_{m=-v}^{N+v-1}x_i(m)h(k-m-i(N+2v))+n(k),\qquad k=-\Delta k+j(N+2v),...,-\Delta k+(N+2v)+N-1. \tag{2.22}$$

It should be noted that, channel convolution operation is integrated with the pre-filtering processes without loss of generality, in Eq.(2.22). $h(k)$ is taken as the general effectual symmetrical channel impulse response subsequent to pre-filter. Using correlation characteristics for $h(k)$, the effectual channel autocorrelation function is denoted as $R(k)=E[h_k,h_k^*]$, and the general correlation function is given by

$$E[h_{k_1},h_{k_2}^*]=[\delta(k_1-k_2)+\delta(k_1+k_2)-\delta(k_1)\delta(k_2)]R(k_1). \tag{2.23}$$

Here, $\delta(k)$ denotes the unit sample sequence, which gives 1 for k = 0 and considered to be 0 for $k\neq 0$. Practically, in a OFDM-based system, the training sequence is generally utilized in the beginning of every symbol in order to estimate the parameters corresponding to imperfections. Such type of mechanism for imperfection detection can be employed in DCT-MCM also. In the subsequent sections, the CFO and TO are assumed to be known through the training symbols.

2.4.2. *Power of Desired Signal, ICI, ISI and Noise*

Because of fading effect resulted from multipath, the DCT output gets corrupted by channel noise plus interference. Here, information symbols are assumed to be statistically independent with mean energy being unity, while transmitted mean energy per symbol is denoted by E_S. At nth output of DCT, power of desired signal may be described in terms of desired signal, ICI, ISI, and colored noise by

$$P_x(n)=E_S\frac{N}{N+2v}(P_U(n)+P_{ICI}(n)+P_{ISI}(n))+V_n. \tag{2.24}$$

The useful power P_U can be attributed to desired symbol $a_{0,n}$. Here, ICI power P_{ICI} denotes contribution from remaining symbols transmitted in intended block (i = 0), while ISI power P_{ISI} represents power from each and every subcarrier within rest of the transmitted blocks ($i\neq 0$).

Eventually, V_n gives contribution from colored noise. By considering the neighboring subcarriers to be modulated, one obtains

$$P_U(n) = E[|\gamma(n,0,n)|^2],$$

$$P_{ICI}(n) = \sum_{l=0,l\neq n}^{N-1} E[|\gamma(n,0,l)|^2],$$

$$P_{ISI}(n) = \sum_{i=-\infty,i\neq 0}^{+\infty}\sum_{l=0}^{N-1} E[|\gamma(n,i,l)|^2], \tag{2.25}$$

where, $\gamma(n,i,l),$ is given by

$$\gamma(n,i,l) = \beta_l\beta_n \sum_{k=0}^{N-1}\sum_{m=-v}^{N+v-1} \cos\frac{\pi(2m+1)(l+\Delta f)}{2N}\cos\frac{\pi(2k+1)n}{2N} h(k-\Delta k - i(n+2v)), \tag{2.26}$$

represents the signalling waveform constituent corresponding to demultiplexed output over n^{th} subcarrier for desired received block *j*=0, resulted from data symbols $a_{i,l}$. These are multiplexed over the *l*th subcarrier having frequency offset Δf taken into account during *i*th communicated block. For distinguishing the signal component from desired as well as interfering subcarriers separately, $\gamma(n,0,n)$ $(i=0, l=n)$ is denoted as power coefficient of desired signalling waveform, whereas the remaining $\gamma(n,i,l)$ represent interfering power coefficients. To calculate constituent $E\left[\left|\gamma(n,i,l)\right|^2\right]$, subsequent to the substitution of Eq.(2.23) in Eq.(2.26), a computationally efficient expression is provided for $E\left[\left|\gamma(n,i,l)\right|^2\right]$ by separating it into six sub-constituents

$$\begin{aligned} E\left|\gamma(n,i,l)\right|^2 = {} & E\left|\gamma_1(n,i,l)\right|^2 + E\left|\gamma_2(n,i,l)\right|^2 + E\left|\gamma_3(n,i,l)\right|^2 + \\ & E\left|\gamma_4(n,i,l)\right|^2 + E\left|\gamma_5(n,i,l)\right|^2 - E\left|\gamma_6(n,i,l)\right|^2, \end{aligned} \tag{2.27}$$

If interfering term for non-synchronized discrete cosine transform MCM system is present, then signal-to-interference ratio (SIR) of n^{th} subcarrier can be expressed as

$$SIR(n) = \frac{P_u(n)}{P_{ICI}(n) + P_{ISI}(n)}. \tag{2.28}$$

This is a well-known fact that discrete cosine transform exhibits energy compaction capabilities. In other words, signal energy is mostly disseminated in the small number of discrete cosine transform coefficients, when rest of the coefficients are considerably low. The DCT operation disseminates large amount of energy to the required subcarrier, while the remaining lower amount of energy is given to ICI than the DFT operation over AWGN channel.

Chapter 3

TWDP AND PHASE NOISE ATTRIBUTES

3.1. Two Wave With Diffuse Power (TWDP)

3.1.1. *Introduction*

Fading is rapid fluctuation of amplitude, phases or multiple delays of a radio signalling waveform over small duration of time or travel distances, ignoring path loss effects up to large extent. It occurs due to the interfering phenomenon of two or more versions of communicated information signalling waveform, which may mix in the destructive or constructive manner at receiving end [30].

In wireless communication, signal propagates through different paths and arrives at receiving end; hence, received signalling waveform is a combination of multipath waves, which are with different phases and amplitudes as in Fig. 3.1. The propagation waves are of two types i.e., specular components and diffuse components. Specular waves are characterized by strong LOS (line of sight) component plus reflected components, while diffuse waves are made up of faint waves with random magnitudes and phases (commonly called scattered components).

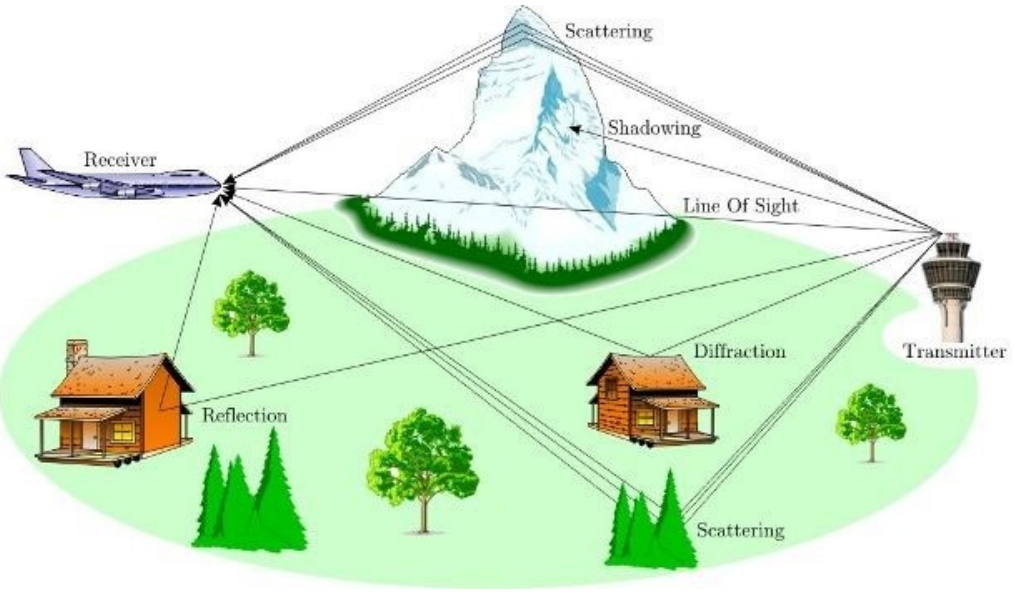

Fig. 3.1. Wireless communication scenario [31].

The resultant signal at the receiver is given as

$$V_r = \sum_{i=1}^{N} V_i \exp(j\phi_i) + \sum_{k=1}^{M} V_k \exp(j\phi_k). \quad (3.1)$$

As given in above equation and represented in Fig. 3.2, received signal is composed of N strong components and M diffuse components. The specular constituent is single term $\{V_i \exp(j\phi_i)\}$, representing an incoming multipath waveform. The phase ϕ_i of the specular constituent is arbitrary, but its envelope V_i is steady. A non-specular-component/diffuse-component, with numerous individual waves carries power which is insignificant to the total average power [26].

TWDP stands for two wave with diffuse power and contains two strong LOS components and many diffuse components. This model has attracted attention, since current wireless scenarios are correctly characterized by this fading model.

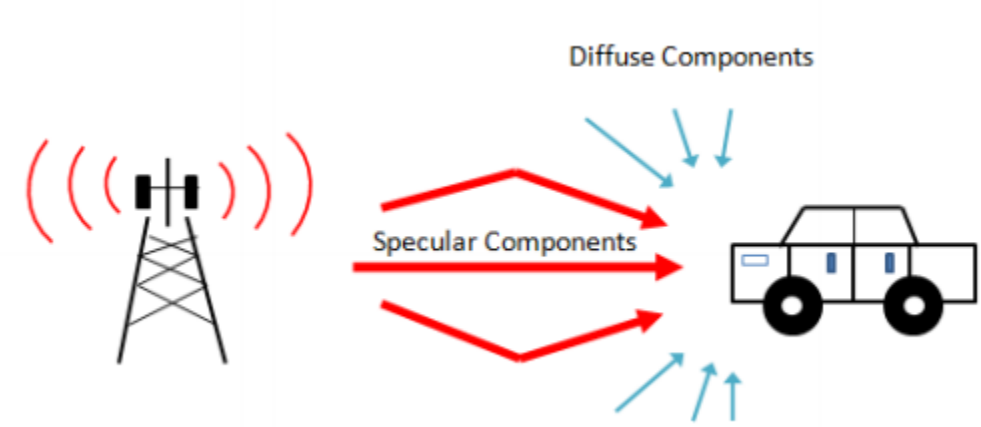

Fig. 3.2. Illustration of specular components and diffuse components [31].

TWDP has two parameters, K and Δ, defined as

$$K = \frac{V_1^2 + V_2^2}{2\sigma^2}, \ \Delta = \frac{2V_1V_2}{V_1^2 + V_2^2}, \quad (3.2)$$

where, V_1 and V_2 are voltage amplitudes of two specular waves; and $2\sigma^2$ denotes mean power of diffused components. K represents specular power's ratio with diffused power, while Δ is two specular component's relative power [26].

Table 3.1 classifies three fading scenarios on the basis of strengths carried by diffuse components and specular components. Table clearly depicts that value of K is negligible in case of Rayleigh fading and is high for TWDP fading environment. Also Δ which is 0.8 for Rician fading approaches 1 in TWDP fading scenario.

Table 3.1. CLASSIFICATION OF FADING ON THE BASIS OF STRENGTHS OF SPECULAR COMPONENTS TO DIFFUSE COMPONENTS [26].

	Example TWDP voltage Values					
CASE	1st Specular Voltage V_1	2nd Specular Voltage V_2	Diffuse RMS voltage $\sqrt{2\sigma^2}$	Value of K	Value of Δ	Type of fading
A	2μV	2μV	3μV	0.89	1	Rayleigh fading
B	4μV	2μV	3μV	2.22	0.8	Rician fading
C	4μV	4μV	3μV	3.56	1	TWDP fading

Rayleigh fading, Rician fading, hyper Rayleigh fading could be considered as the special cases of TWDP fading. When K=0, TWDP fading model deteriorates to Rayleigh; for Δ=0, Rician fading is approximated; and when Δ≈1 and $K\rightarrow\infty$, hyper Rayleigh fading comes into action. Fig. 3.3 represents specular and diffuse components in TWDP fading.

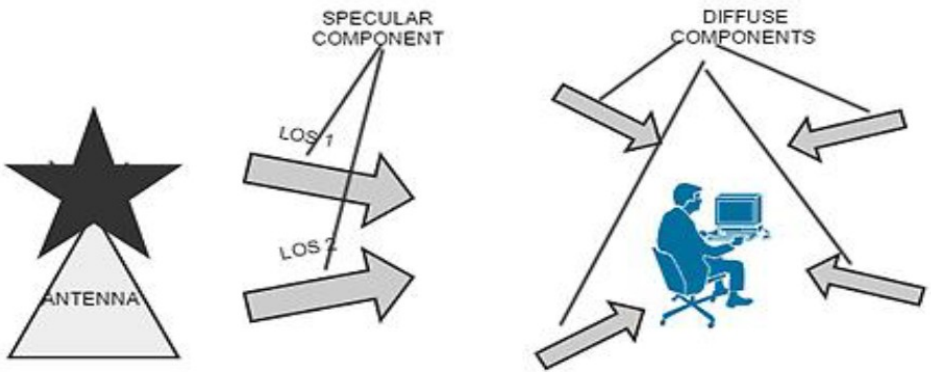

Fig. 3.3. TWDP environment with two specular components and many diffuse components [31].

TABLE 3.2. RANGE OF VALUES OF K AND Δ TO CLASSIFY THE TYPE OF FADING [26].

Type of Fading	Value of K	Value of Δ
Rayleigh fading	-∞ to 0dB	Not applicable
Rician fading	1 to 3 dB	Δ=0
TWDP fading	3 to ∞ dB	Δ=0 to 1

3.1.2. *Why TWDP Fading Scenario is Important to Study?*

It has been proved in [32] that when two LOS components are alike in magnitude and opposite in phase on reaching receiver side, a link is produced, which is even worse than Rayleigh fading. Rayleigh fading model has till now been considered to design worst case wireless communication system, but this new study has limited the use of Rayleigh model and proposed the use of TWDP fading model to design wireless communication systems. Also the use of directional antennas, wideband signals and typical narrowband receiver operations increases the probability of occurrence of TWDP fading [26].

TWDP fading comes into action, when power of specular components is much greater than power of diffuse components i.e., value of parameter K is high. Both directional antennas and wideband signals give rise to these conditions. Directional antennas amplify one multipath wave that is in a particular direction, while the remaining signal is attenuated. Even wide band signal reception do the same, it rejects multipath signalling constituents which arrive at different time delays. Hence, this automatically increases the strength of specular component in comparison to diffuse waves [26].

Current wireless systems have made their implementation possible almost everywhere. Wireless sensor networks are deployed in cavity environments for instance airframes as well as shipping containers. The propagation environment within these cavities is comparatively static and does not possess capability to fight fades. Hence, new worst case model to correctly characterize this environment space needs to be studied.

3.2. Phase Noise

3.2.1. *Introduction*

The oscillator may be regarded as the filtered noise generator, thus noise will be surrounding carrier, similar to arbitrary AM and FM modulations over ideal RF sinusoidal wave, such supplementary noise can be referred to as phase noise. In case, anybody takes into account accumulation of the noise voltage to the sine voltage, then the phase relationship must also be taken into account. Noise includes components of numerous frequencies, therefore it has an arbitrary phase as well as amplitude with respect to the main carrier.

In local oscillator (LO) of transmitter noise, amplification is through the successive amplifier stages, which is further fed to an antenna collectively along with desired signalling waveform. Here, desired information signalling waveform is thus bounded with the band of noise which is result of phase noise from LO. As a result, the noise produced is capable of spreading over

several kHz masking nearby low power stations. The scenario is further complex for the receivers which allows reciprocal mixing of mixer. On modulating the radio frequency (RF) signalling waveform and then, mixing it with the local oscillator resource will result in the modulated intermediate frequency (IF) signalling waveform. If clean RF signalling waveform is mixed with the modulated LO resource, then it will result in a modulated IF. The modulation will appear to be the same to the listener. This result can be demonstrated by implying that the noise components can be referred as additional LOs that have an offset from the key carrier. Each noise component combines with other signalling waveforms with offset from LO through IF receiving configurations. Noise can be termed as the sum of an infinite number of infinitesimal constituents spreading over wide frequency range, so that signalling waveform which it mixes into intermediate frequency is spread onto the infinite number of small replicas, each and every one at various frequencies. It leads to the mixing up of the other weak frequencies into noise. This is main reason behind PHN being the vital design criterion for such applications like sensitive communication receiving configurations, satellite repeaters as well as cell phone base stations.

PHN ought to be critically contemplated while dealing with any communication system because a precise projection of the bearable PHN may let system as well as RF designers to relax specifications. The effects of PHN introduced due to LO in the receiving configuration may only be improved by ameliorating capability of oscillator itself, with an increase in related price. Therefore, it is important to determine the extent of PHN, a receiver may bear up while exhibiting desired output. PHN may be considered as the parasitic phase modulation in oscillator's signalling waveform, which preferably would be the unique carrier with constant amplitude as well as frequency.

OFDM is extremely responsive to PHN originating from imperfect realistic oscillators. Numerous techniques were presented in order to lessen consequences of PHN in orthogonal frequency division multiplexing receiving configuration. These techniques are proficient in compensating for PHN, however such techniques can deteriorate bandwidth efficiency, as pilot information signals are utilized.

3.2.2. *Brief Details About Wiener Phase Noise in IDFT/DFT Based Systems*

The bits of OFDM modulated signalling waveforms are generated by performing IDFT of a discrete-time input data sequence $\{a_i\}$ and then, using a pulse-shaping filter on transform bits. Here, dual transformations have to be carried out at the receiver end.

After frequency down-conversion and by assuming an additive white Gaussian noise (AWGN) channel, received signalling waveform may be represented like

$$u(t) = [r(t) + n(t)]\varepsilon(t), \tag{3.3}$$

where, $r(t) \triangleq \sum_{k=0}^{N-1} a_k e^{j2\pi k\frac{t}{T}}$ ($j = \sqrt{-1}$), $n(t)$ denotes the additive noise, while $\varepsilon(t) \triangleq e^{j\vartheta(t)}$ represents the multiplicative error term as a result of oscillator PHN. Here, PHN $\vartheta(t)$ may be assumed as the continuous path Brownian motion having zero average and variance $2\pi\beta|t|$ (parameter β indicates two-sided 3-dB linewidth of the oscillator's Lorentzian power density spectrum). This presented mathematical paradigm is sufficiently precise for modelling PHN process, also apt for getting a quantitative measure of degradation in system output because of PHN. Nonetheless, it has to be taken into account that this technique is applicable only if the baseband conversion of orthogonal frequency division multiplexing signalling waveforms is carried out by the free-running oscillator. As an alternative, if baseband conversion is carried out by the using the oscillator in appropriately locked state with carrier of received signalling waveform, then phase error variance increases within limit.

At receiving side, signalling waveform $u(t)$ is multiplied by subcarriers having same frequency at the transmitter side and passed to N integrate-and-dump (I&D) filtering configurations with integration time. As a result, output signal of ith I&D filter is

$$z_i = a_i\lambda_0 + \sum_{\substack{k=0 \\ k\neq i}}^{N-1} a_k\lambda_{i-k} + \eta_i, \qquad 0 \le i < N \tag{3.4}$$

where,

$$\lambda_k \triangleq \frac{1}{T}\int_0^T e^{j\left\{\vartheta(t) - 2\pi k\frac{t}{T}\right\}} dt, \tag{3.5}$$

and η_i denotes the samples of AWGN. In Eq.(3.4) the information quantity a_i is multiplied by λ_0, which relies on the phase noise, however it is not dependent on any particular subcarrier index. The summing term in Eq.(3.4), instead, signifies the interbin interference that is zero for $\vartheta(t) = 0$. Note that such interference is dependent on information symbols pertaining to every subcarriers.

For BPSK, the decision variable for the ith subcarrier is expressed as

$$z_i = a_i\lambda_0 + \zeta_i + \eta_i, \qquad \zeta_i \triangleq \sum_{\substack{k=0 \\ k\neq i}}^{N-1} a_k\lambda_{i-k}, \qquad a_i = \{\pm 1\}. \tag{3.6}$$

where,

$$\lambda_0 \triangleq \lambda_{0R} + j\lambda_{0I} = \frac{1}{T}\int_0^T e^{j\vartheta(t)}dt. \tag{3.7}$$

When $\gamma < 0.5$, the exponential function in Eq.(3.7) can be represented in power series as $e^{j\vartheta(t)} \simeq 1 + j\vartheta(t)$. The joint moment generating function (MGF) of the real as well as imaginary parts of Eq.(3.7) is given by

$$\xi_{\lambda_{0R}\lambda_{0I}}(s_1, s_2) = \frac{e^{s_1}}{\sqrt{\cosh\sqrt{\gamma s_1}}} \exp\left\{\frac{\gamma}{2}\left(\frac{s_2}{2}\right)^2\left[\tanh c\sqrt{\gamma s_1} + \coth c\sqrt{\frac{\gamma s_1}{4}} - \frac{4}{\gamma s_1}\right]\right\}. \tag{3.8}$$

$$\exp\left\{-\frac{\gamma^2 s1}{2}\tanh c\sqrt{\gamma s_1}.\left[s_2\left(\coth c\sqrt{\gamma s_1} - \frac{1}{\gamma s_1}\right)\right]^2\right\}$$

where, $\gamma \triangleq 2\pi\beta T$, $\cot ca \triangleq \frac{\coth a}{a}$, and $\tanh ca \triangleq \frac{\tanh a}{a}$. Nonetheless, it is difficult to get the statistics of ζ_i. Due to this reason, ζ_i is approximated as the complex Gaussian RV (RV) with average as well as variance as

$$\mathfrak{M}_{\zeta i} \triangleq E[\zeta_i] = \sum_{\substack{k=0 \\ k\neq i}}^{N-1} E[a_k]E[\lambda_{i-k}] = 0, \tag{3.9}$$

and

$$\sigma_{\zeta i}^2 \triangleq E[|\zeta_i - \mathfrak{M}_{\zeta i}|^2] = \sum_{\substack{k=0 \\ k\neq i}}^{N-1} E[|a_k|^2]E[|\lambda_{i-k}|^2], \tag{3.10}$$

respectively. On utilizing the Smirnov test, through simulations it has been verified that significance levels are, roughly, between 0.7–0.9. As a result, $\Im_i \triangleq \zeta_i + \eta_i$ is the zero-average Gaussian RV having variance $\sigma_{\zeta i}^2$ and bit-error-rate as

$$BER = \frac{1}{2}\left\{P\left[\Re[z_i] < 0 \,|\, a_i = +1\right] + P\left[\Re[z_i] \geq 0 \,|\, a_i = -1\right]\right\}. \tag{3.11}$$

Every term in between curved brackets of Eq.(3.11) can be evaluated with the help of MGF of the RV involved

$$P\left[\Re[z_i] < 0 \,|\, a_i = +1\right] = -\frac{1}{2\pi j}\int_{-j\infty+v}^{j\infty+v} \frac{\xi_1(s)}{s}ds, \qquad v < 0. \tag{3.12}$$

In Eq.(3.12), $\xi_1(s)$ is the MGF of $\Re[z_i]$ conditional to $a_i = +1$, namely

$$\xi_1(s) = E\left[e^{s\{\Re[\lambda_0 + \Im_i]\}}\right] = E\left[e^{s\{\lambda_{0R} + \Im_{iR}\}}\right] = \xi_{\lambda_{0R}}(s)\xi_{\Im_{iR}}(s) \tag{3.13}$$

where,

$$\xi_{\lambda_{0R}}(s) = \frac{e^s}{\sqrt{\cosh\sqrt{\gamma s}}}, \qquad \xi_{\Im_{iR}}(s) = \exp\left\{\frac{1}{2}\sigma^2_{\Im_{iR}} s^2\right\}, \quad \gamma \triangleq 2\pi\beta T. \tag{3.14}$$

The saddlepoint approximation is an accurate as well as fast method to evaluate integrals like Eq.(3.12).

3.2.3. *PHN Generation* [35]

The phase noise process $\{\varphi_i\}$ may be modelled like the wiener process or a continuous Brownian motion, and φ_i may be represented as

$$\varphi_i = \varphi_{i-1} + u_i, \quad 0 \le i \le N-1, \tag{3.15}$$

where, u_i denotes the independent increments in PHN at the time instant i with Gaussian distribution with zero-average and variance σ^2_{PN} .Here, φ_{-1} can be set 0 at the beginning of the OFDM data symbol due to perfect synchronization.

3.2.4. *Impact of Phase Noise, Frequency Offset, and I/Q Imbalance on IDFT/DFT Based System* [4]

Variations in the local oscillator's (receiver side) phase and frequency and difference in the received signal's carrier can deteriorate the performance of the system. OFDM's drawbacks are typically categorized in terms of its source, for instance, Doppler spread in the channel, local oscillator's frequency offset between transmitting side and receiving side, and various PHN paradigms having properties which are dependent on carrier recovery mechanisms at the receiver. These outcomes are generally indirectly valid for optical applications of OFDM.

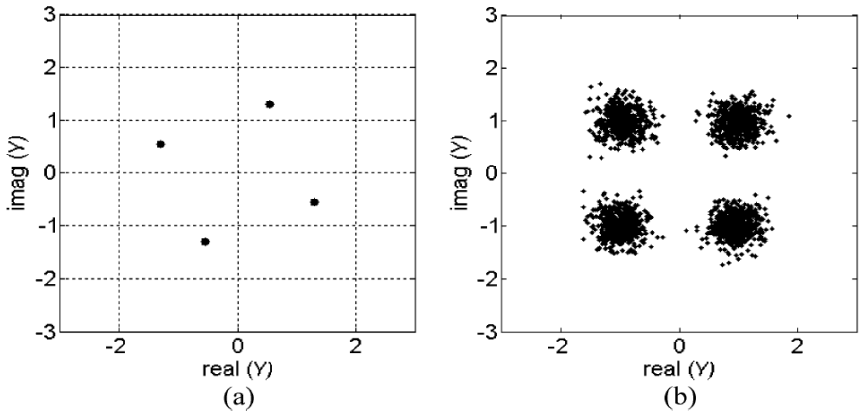

Fig. 3.4. Effects of phase error on received OFDM signal-space configuration

(a) when phase error is static $\theta_m = \theta_0 = \pi/8$ and

(b) when PHN is uncorrelated and $E\{\theta_m^2\} = 0.05\ rad^2$ [4].

Consider the case where the channel is distortion free, and $\varphi_d = 0$, so that I/Q phase imbalance is not there. Then utilizing the products and sums formulae for angles along with some simple manipulations, the samples of received time domain signal are represented as

$$y_m = x_m \exp(j\theta_m), \tag{3.16}$$

where, θ_m denotes the phase error at receiving end for m^{th} sample of orthogonal frequency division multiplexing symbol under analysis.

In case, when phase error is static, i.e., $\theta_m = \theta_0$, implies that $y_m = x_m \exp(j\theta_0)$, and it is simple to show that

$$Y_k = \exp(j\theta_0) X_k. \tag{3.17}$$

The signal-space configuration gets simply rotated by angle θ_0. A typical example is demonstrated in Fig. 3.4(a). In the orthogonal frequency division multiplexing system, it would be automatically corrected in single-tap equalization approach.

Subsequently, considering opposite extreme, when phase noise has zero-average, and phase noise samples are uncorrelated to each other $E\{\theta_m \theta_n\} = 0, m \neq n,$ where $E\{\ \}$ illustrates expectation operator.

Further, by performing FFT operation, it can be shown that

$$\begin{aligned} Y_k &= \frac{1}{\sqrt{N}} \sum_{m=0}^{N-1} y_m \exp\left(\frac{-j2\pi km}{N}\right) \\ &= \frac{1}{\sqrt{N}} \sum_{m=0}^{N-1} x_m \exp(j\theta_m) \exp\left(\frac{-j2\pi km}{N}\right). \end{aligned} \tag{3.18}$$

For small phase error, utilizing the small angle approximation $\exp(j\theta_m) \approx 1 + j\theta_m$

$$\begin{aligned} Y_k &= \frac{1}{\sqrt{N}} \sum_{m=0}^{N-1} x_m (1 + j\theta_m) \exp\left(\frac{-j2\pi km}{N}\right) \\ &= X_k + \frac{1}{\sqrt{N}} \sum_{m=0}^{N-1} j\theta_m x_m \exp\left(\frac{-j2\pi km}{N}\right) \\ &= X_k + \mathrm{Z}_k. \end{aligned} \tag{3.7}$$

The demodulated subcarrier Y_k represents the transmitted subcarrier in addition to the noise like component, Z_k, and it is dependent on every transmitted subcarrier. Statistical independence of θ_m as well as x_m helps to calculate the power of Z_k, Fig. 3.4(b).

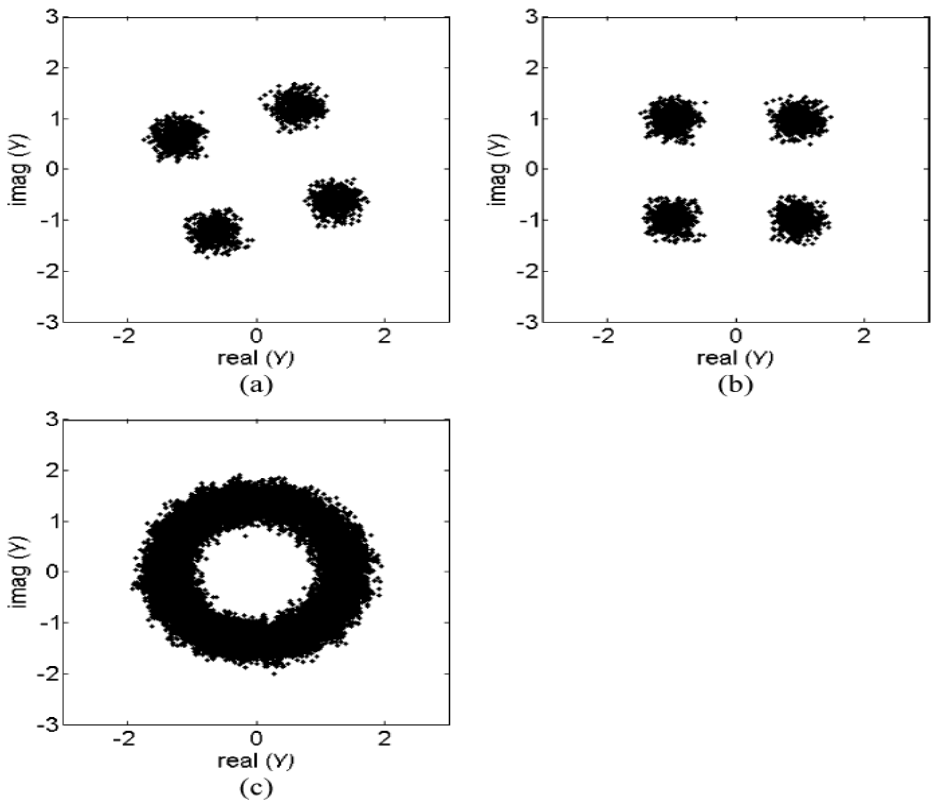

Fig. 3.5. Effects of frequency offset $\Delta fT = 0.2$ on received signal-space configuration

(a) phase offset zero at start of every OFDM symbol,

(b) phase offset zero in middle of every OFDM symbol, and

(c) no phase offset rectification [4].

For θ_m with attributes inbetween such extremes, phase error leads to a combination of noises like ICI as well as constellation rotation, also sometimes referred to as common phase error. For instance, if the frequency offset between transmitting end and receiving end is fixed, such that $f_r = f_c + \Delta f$, then phase variations occur in linear mode with time $\theta(t) = \Delta ft$. It leads to the continuously rotating constellation as well as a noise-like term. The resulting system BER depends upon the phase tracking process of receiver. If in the phase tracking process $\theta(t) = 0$ at starting of every symbol period, then received signal-space configuration has the form depicted in Fig. 3.5(a). If receiver predicts change in phase, then signal-space configuration exhibits a form depicted in Fig. 3.5(b). In the case of no correction or tracking, the constellation rotates continuously with no useful information to transfer. See Fig. 3.5(c). It has been found that in CO-OFDM systems, deleterious effect of phase noise may be reduced by inserting pilot tones within OFDM symbol, and further utilizing such tones for tracking variation in laser PHN.

3.2.5. *Effect of PHN on OFDM* [33]

Assuming perfect timing and frequency synchronization, i.e., only considering PHN, received *n*th sample of *m*th orthogonal frequency division multiplexing symbol is given by

$$r_m(n) = x_m(n) \otimes h_m(n).e^{j\varphi_m(n)} + \xi_m(n), \tag{3.8}$$

where, $x_m(n)$, $\varphi_m(n)$ and $h_m(n)$ indicate transmitted signalling waveform, phase noise and channel-impulse response, respectively, while $\xi_m(n)$ represents AWGN noise having variance σ^2. After eliminating cyclic prefix, and performing discrete Fourier transform operation, resultant frequency-domain signal can be expressed as

$$R_m(k) = X_m(k)H_m(k)I_m(0) + \sum_{l=-N/2}^{N/2-1} X_m(l)H_m(l)I_m(l-k) + \zeta(k), \tag{3.9}$$

where, $X_m(k), H_m(k)$ and $\zeta_m(k)$ are related frequency-domain expressions of $x_m(n), h_m(n)$ and $\xi_m(n)$ respectively. $I_m(i)$ is a function of $\varphi_m(n)$ defined as

$$I_m(i) = \frac{1}{N}\sum_{n=-N/2}^{N/2-1} e^{j2\pi ni/N} e^{j\varphi_m(n)}, \qquad i = -\frac{N}{2},...,\frac{N}{2}-1. \tag{3.10}$$

From Eq.(3.9), we observe that besides common phase error (CPE) or phase rotation of the desired sample, random phase noise also causes ICI. Therefore, it deteriorates the performance of the receiver.

The second term in Eq.(3.9) indicates ICI, which is a RV independent of $\zeta_m(k)$. $X_m(k)$ can be considered as mutually independent random variables which does not depend on $H_m(k)$ with zero average and variance E_x. Hence, ICI term in Eq.(3.9) has a zero mean.

Chapter 4

IDCT/DFT BASED COMMUNICATION SYSTEM WORKING IN THE PRESENCE OF PHASE NOISE

4.1. Introduction

Fast–orthogonal–frequency–division–multiplexing (F–OFDM) system has emerged as a proficient multicarrier (MC) transmission scheme, in which the subcarrier spacing is half of that of the traditional OFDM scheme [10]–[12]. In the domain of fiber optic communication systems, the discrete–cosine–transform (DCT) is usually preferred over discrete–Fourier–transform (DFT) in F–OFDM systems for information symbol multiplexing onto the subcarriers [13]–[15]. Exclusively, F–OFDM possesses enhanced tolerance, to the carrier frequency offset in optical coherent detection, as well as to the Doppler shift in wireless communication [16], [17]. However, F–OFDM exhibits better receiver sensitivity in optical full field detection [18]. These striking features make the F–OFDM technique an efficient and suitable technique for MC transmission. But, one of the key challenges in optical communication systems utilizing DCT based F–OFDM technique is that the DCT exhibits symmetric convolution property [19], in which two sequences must be symmetrically extended to make the DCT of convolution equal to the product of their individual DCTs. This imposes a stringent condition that the symmetric prefix as well as suffix are needed as guard-interval (GI) for F–OFDM signaling in addition to the inherently symmetric channel–impulse–response (CIR). Here, single-tap equalization in the cosine–domain for F–OFDM signaling for the symmetric channels is promising only under a few typical cases like chromatic dispersion in the single-mode-fiber (SMF) optic channel [20].

On the contrary, under generic linear fading channel conditions (like modal dispersion in multi-mode-fibers (MMF) optic channel and multipath fading in wireless channel), the condition for symmetric convolution is not fulfilled, and it precludes the usage of traditional single-tap equalizers for CIR compensation. The condition of symmetric convolution can be met by symmetrically extending the F–OFDM signal, but it is possible at the cost of reduced data-rate [21]. Subsequently, the minimum-mean-square-error (MMSE) criterion based time-domain pre-filtering at the receiver is suggested in [22] to improve the data-rate under similar conditions. But, its major limitation is computational complexity. Further, in frequency-domain-equalization

(FDE) [23], the CIR impairments are compensated at the receiver (using DFT operations) before the signal is transformed to cosine-domain by using DCT operation. However, it is observed that noise in the frequency-domain is getting amplified, and it is found to spread over the subcarriers after DCT operation. Though the MMSE criterion based equalizer performs well as compared to the zero-forcing (ZF) equalizer in controlling this noise amplification, but the underlying F–OFDM system still appears to be vulnerable to the noise at spectral nulls [36].

Ouyang *et al*. [37] have reported a low complexity F–OFDM scheme for generic linear fading channels (like modal dispersion in MMF optic channel [38] and multipath fading in wireless channel), which can be employed for the single-tap equalization irrespective of the requirement of symmetric channel characteristics. This technique outperforms the FDE based F–OFDM technique working under the frequency–selective channels. It compensates generic linear-time-invariant (LTI) channels by utilizing a single-tap equalizer without compromising data-rate. In addition to zero-padded (ZP) GI, the DFT of double length (*i.e.*, 2N–point) has been incorporated at the receiver instead of the conventional N–point DCT approach; where N is number of demultiplexed subcarriers. However, MC modulation possesses a substantial sensitivity to the phase-noise (PHN) of oscillator utilized for frequency down-conversion at receiving end [34], which causes interbin interference (depending on the information data from all of the different subchannels).

Moreover, orthogonal frequency division multiplexing systems are sensitive to PHN and to carrier-frequency-offset (CFO), respectively, caused by the oscillator imperfections as well as Doppler shifts [4], [39], [40]. Indeed, these phase distortions disturb the orthogonality of OFDM subcarriers, and it results both in rotation of every subcarrier by a random phase, known as common-phase-error (CPE) [33], and to inter-carrier-interference (ICI). The performance of underlying OFDM system gets deteriorated due to the presence of this random Wiener phase noise, which also significantly degrades the efficiency of channel estimator [41]. The effects of Wiener phase noise has been examined by Pollet *et al*. in [39], which have been found to be a much more complex phenomenon as compared to CFO. The PHN generated by the fluctuations of receiver as well as transmitter oscillators causes leakage of DFT [42]. The CPE causes subcarrier phase rotation, which doesn't vary within OFDM symbol duration; while ICI introduces interference to any subcarrier of a certain symbol from all other subcarriers of that symbol, and therefore it possesses noise-like features. However, the higher PHN levels are catastrophic, as these make ICI dominant over the transmitted signalling waveform [43]; but the lower phase noise levels can be tackled by estimating as well as compensating for common-

phase-error, only by minimizing mean-squared-error (MSE) [44], [45]. To better characterize PHN, Demir *et al*. [46] reported a unifying theory by utilizing a nonlinear scheme, which proves to be quite accurate as per its details. Here, the phase noise $\phi(t)$ is illustrated to become (asymptotically in time) a Gaussian random process having a constant average, a variance increasing linearly with time and the correlation function that satisfies $E\left[\phi(t)\phi(t+\tau)\right] = Min\left[E\left\{\phi^2(t)\right\}, E\left\{\phi^2(t+\tau)\right\}\right]$. Nikitopoulos *et al*. have indicated in [47] that a discrete Markov-process is an appropriate model to illustrate PHN.

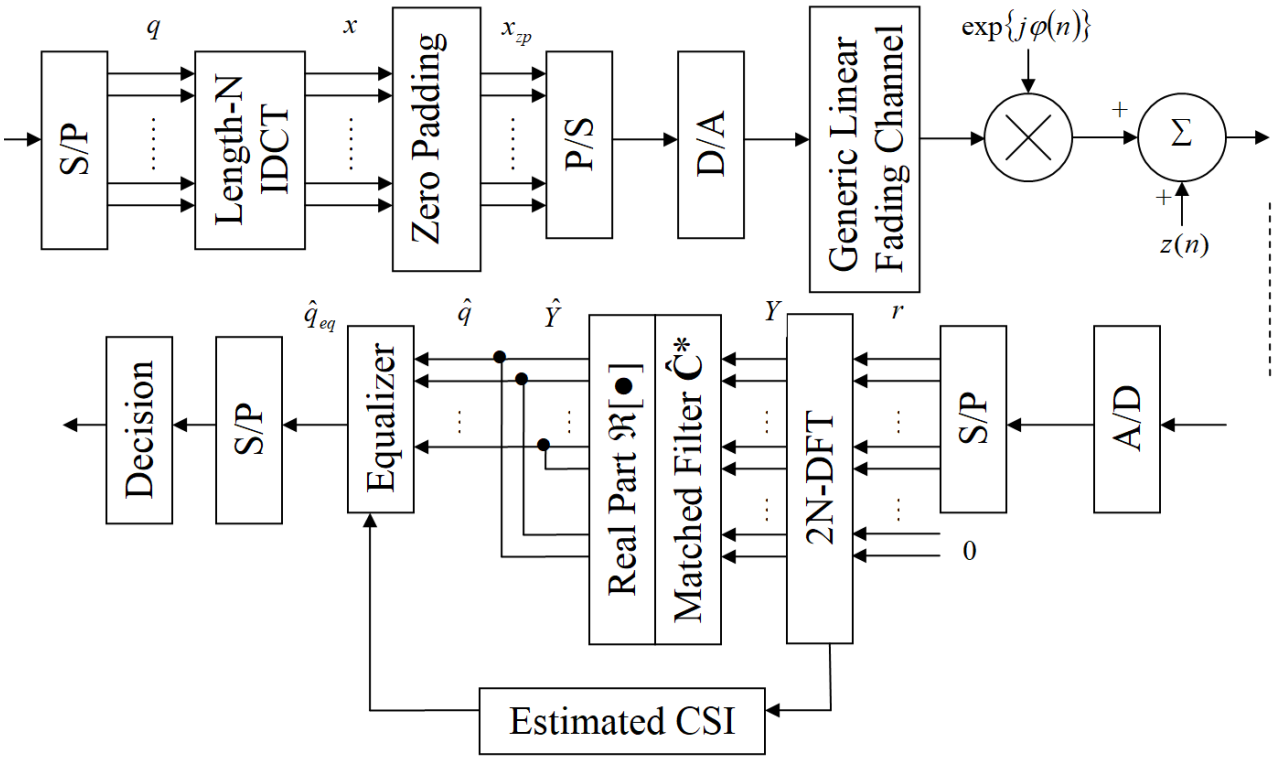

Fig. 4.1. Block diagram of fast–OFDM system with single-tap equalizers working in the presence of PHN.

The small scale fading encountered by the narrowband receivers has been extensively explored by characterizing fading channels, while utilizing the Rayleigh, Rician or Nakagami-m probability density functions (PDFs) [26], [48], where the complexity of analysis is quite less than that of the two-wave-with-diffuse-power (TWDP) fading for phase modulation schemes. Actually, TWDP is characterized by the presence of multiple scattered waves and two line-of-sight components with constant amplitudes and uniformly as well as independently distributed phases [26], [49], which can also be represented as an infinite mixture of gamma distributions

[50]. The recent studies in this field quantitatively reveal that TWDP fading can give rise to a link worse than Rayleigh fading, when two direct waves are found to be equal in strength, but opposite in phase, and exhibit a combined power of $\geq 6dB$ higher than diffused power. This inference points towards the utilization of TWDP fading rather than Rayleigh fading as a worst case scenario in designing and evaluating the wireless transmission systems [51]. To address this issue in the domain of F–OFDM signal transmission and reception, the performance of single-tap ZF equalization technique needs to be investigated further.

In this research work, we emphasis on the performance evaluation of an efficient F–OFDM technique using the IDCT operation at transmitter and the DFT operation at receiver [37], in the presence of phase noise [41], [43], while working under the generic linear fading channels (like TWDP fading channels [26], [50], [51], in which the requirement for symmetric condition is not satisfied in underlying system). In Section 4.2, we describe the F–OFDM communication system affected by PHN, which uses a ZF equalization based approach for the CIR compensation. The details about phase noise attributes are provided in Section 4.3. Simulation results are presented in Section 4.4 to illustrate average BER output of F–OFDM system under the influence of PHN, and to analyze the adverse impact of PHN variations on its BER at the different values of signal-to-noise-ratio (SNR).

4.2. F-OFDM System Working Under Linear Fading Channel and Phase Noise

A paradigm for the F–OFDM system working under the linear generic fading channel, in the presence of phase noise, is illustrated in Fig. 4.1. The *kth* subcarrier is modulated by the information symbols $q[k]$, when there are N subcarriers with $k = 0,1,.....,N-1$. The related time-domain signalling waveform samples $x(n)$ are generated by using the inverse-DCT (IDCT) operation [25], it follows that

$$x(n) = \sqrt{2/N}\sum_{k=0}^{N-1} \varepsilon[k]\, q[k] \cos\{\pi k (n+0.5)/N\} \qquad \text{for } n = 0,1,.....,N-1 \tag{4.1}$$

where, $\varepsilon[k] = \sqrt{1/2}$ for $k = 0$, and 1 for $k = 1,.....,N-1$. To suppress the deleterious effects of inter-symbol-interference (ISI), the zero-padding strategy is utilized in place of symmetric prefix and suffix based guard interval [19], [20]. Ouyang *et al*. [37] have reported that ZP based GI scheme performs well when single-tap equalizers are incorporated for CIR compensation under

the generic linear-time-invariant (LTI) channel scenario, such that $x_{zp}(n) = x(n)$ for $0 \le n \le N-1$, and $x_{zp}(n) = 0$ for $N \le n \le N+L-1$; where L is the length of generic linear fading channel (multipath in nature *i.e.*, L is equivalent to the number of filter tap-coefficients in a tapped-delay-line filter [48], [52]). The impulse response of multipath fading channel in continuous-domain is $c(t) = \sum_{l=0}^{L-1} c_{\tau l}(t)\delta\left(t - \tau_l(t)\right)$ with *lth* tap-coefficient $c_{\tau l}(t)$ with respective delay $\tau_l(t)$. In discrete-domain, $\tau_l(t)$ is assumed to be an integer multiple of information symbol duration T_s, such that $c(n) = \sum_{l=0}^{L-1} c_{l;n}\delta(n-l)$ with *lth* tap-coefficient $c_l = c_{l;n}$ and Dirac delta function δ. For chromatic dispersion in a SMF, $c(n)$ is symmetric; whereas it is non-symmetric in MMF channels and in wireless multipath propagation. Here, $c(n)$ is considered to be complex for the multipath wireless fading channel. Based on Eq.(4.1), the received signal in the presence of phase noise $\phi(n)$ is mathematically modelled as

$$r(n) = \left\{c(n) * x_{zp}(n) + w(n)\right\} e^{j\phi(n)} = x_{zp}(n) * \left\{c(n)e^{j\varphi(n)}\right\} + z(n) \tag{4.2}$$

where, $z(n) = w(n)e^{j\phi(n)}$ (with $\phi = \varphi$; as both models are same [33], [34]), "$*$" is convolution operator, $w(n)$ is the zero-average additive-white-Gaussian-noise (AWGN) and variance σ_w^2. The above equation can be rewritten as

$$r(n) = x_{zp}(n) * h(n) + z(n) \qquad \text{for } 0 \le n \le N+L-1 \tag{4.3}$$

where, $h(n) = c(n)e^{j\phi(n)}$ (as shown in Fig. 4.1), and the white noise samples $z(n)$ in Eq.(4.3) are also found to possess zero-mean with variance σ_w^2. The multiplication of $e^{j\phi(n)}$ with $w(n)$ further randomizes AWGN samples. Subsequently, the zero-padding is performed to incorporate zeros in the end of received signal $r(n)$ to obtain $r_{2N}(n)$ with length $2N$. Therefore, instead of DCT operation, a $2N$-point DFT operation $F_{2N}[\bullet]$ is performed by utilizing ZP to attain the frequency-domain signal $Y[m]$ *i.e.*,

$$Y[m] = \left\{C[m]X[m]\right\} \otimes J[m] + Z[m] \qquad \text{for } m = 0, 1, ..., 2N-1 \tag{4.4}$$

where, "$\otimes$" is the circular convolution operator, and $F_{2N}[\bullet]$ indicates the normalized DFT operation of length $2N$-point. In above equation,

$$C[m] = \sum_{l=0}^{L-1} c_l \exp\left[\frac{-j2\pi lm}{2N}\right] \tag{4.5}$$

$$J[m] = \frac{1}{2N}\sum_{n=0}^{2N-1} \exp\{j\phi(n)\} \exp\left[\frac{-j2\pi nm}{2N}\right] \tag{4.6}$$

Here, $J[0]$ is commonly known as common-phase-error (CPE), which relates to time-average $\frac{1}{2N}\sum_{n=0}^{2N-1} \exp\{j\phi(n)\}$ [4], [43]. The Eq.(4.4) can also be expressed as

$$Y[m] = C[m]X[m]J[0] + Z\Gamma[m] \tag{4.7}$$

where,

$$Z\Gamma[m] = Z[m] + \Gamma[m] \tag{4.8}$$

and

$$\Gamma[m] = \sum_{i=0;i\neq m}^{2N-1} C[i]X[i]J[m-i] \quad \text{(ICI - term)} \tag{4.9}$$

It can be inferred from Eq.(4.7) that PHN distorts $Y[m]$ in a multiplicative trend via CPE-term $J[0]$, and in an additive manner via ICI-term $\Gamma[m]$, Eq.(4.9) [33]. The Eq.(4.6) can be further simplified as

$$J[m] \approx \frac{1}{2N}\sum_{n=0}^{2N-1} \{1 + j\phi(n)\} \exp\left[\frac{-j2\pi nm}{2N}\right] \tag{4.10}$$

Using Eq.(4.10), the approximate value of CPE-term is observed to be

$$J[0] \approx 1 + j\theta[0] = 1 + \frac{j}{2N}\sum_{n=0}^{2N-1} \phi(n) \tag{4.11}$$

Here, $\theta[0]$ is the angle resulting due to the average phase noise in $2N$ samples, which accounts for the rotation of signal constellation [43]. Therefore, PHN has deleterious/adverse effects on the performance of F–OFDM system. For further analysis, Eq.(4.7) can be represented as

$$Y[m] = \left\{\exp\left(+\frac{j2\pi m}{2N}0.5\right)C[m]\right\}\left\{\exp\left(-\frac{j2\pi m}{2N}0.5\right)X[m]\right\}J[0] + Z\Gamma[m] \tag{4.12}$$

or

$$Y[m] = \left\{\hat{C}[m]\right\}\left\{\hat{X}[m]\right\}J[0] + Z\Gamma[m] \tag{4.13}$$

where,

$$\hat{X}[m] = \sqrt{\frac{1}{2N}} \sum_{n=0}^{N-1} x(n) \exp\left(\frac{-j2\pi m(n+0.5)}{2N} \right) = \sum_{k=0}^{N-1} q[k] P(m,k) \,, \tag{4.14}$$

and $P(m,k)$ [37] is denoted as

$$P(m,k) = \frac{\varepsilon[k]}{N} \sum_{n=0}^{N-1} \cos\left\{ \frac{\pi}{N} k\left(n+0.5\right) \right\} \exp\left(\frac{-j\pi m}{N} \left(n+0.5\right) \right) \tag{4.15}$$

Its real part is skew-symmetrical around N . It follows that

$$P_R(m,k) = \frac{\varepsilon[k]}{N} \sum_{n=0}^{N-1} \cos\left\{ \frac{\pi}{N} k\left(n+0.5\right) \right\} . \cos\left\{ \frac{\pi}{N} m\left(n+0.5\right) \right\} \tag{4.16}$$

or, $P_R(m,k) = \begin{cases} +1.0 & m = 0 \\ +0.5\ \delta(m-k) & m = 1,....., N-1 \\ 0 & m = N \\ -0.5\ \delta(2N-m-k) & m = N+1,....., 2N-1 \end{cases}$

To detect the transmitted information symbol at receiver, the channel frequency response $\hat{C}[m]$ is stringently required, which can be estimated by utilizing a number of adaptive channel estimation algorithms [52]–[55] depending on the properties of channel. To recover transmitted information symbols $q[m]$, the following operation is performed on Eq.(4.13) to obtain

$$\hat{Y}[m] = \hat{C}^*[m] Y[m] \tag{4.17}$$

By using Eqs.(4.7), (4.14) and (4.16), the above equation can be simplified as

$$\hat{Y}[m] = \left| \hat{C}[m] \right|^2 J[0] \sum_{n=0}^{N-1} q[k] P_R(m,k) + \hat{C}^*[m] Z\Gamma[m] \tag{4.18}$$

$$= \hat{C}^*[m] Z\Gamma[m] + \left| \hat{C}[m] \right|^2 J[0] \begin{cases} +1.0q[m] & m = 0 \\ +0.5q[m] & m = 1,..., N-1 \\ 0 & m = N \\ -0.5q[2N-m] & m = N+1,..., 2N-1 \end{cases}$$

where, $(\ )^*$ is complex conjugate operator. Simplification using Eqs.(4.13), (4.17) and (4.18) results in

$$\hat{q}[m] = \hat{Y}[m] - \hat{Y}[2N-m] = \hat{C}_c[m] J[0] q[m] + \eta[m] \tag{4.19}$$

where,

$$\hat{C}_c[m] = 0.5\left\{\left|\hat{C}[m]\right|^2 + \left|\hat{C}[2N-m]\right|^2\right\} \tag{4.20}$$

and

$$\eta[m] = \overline{Z\Gamma}[m] - \overline{Z\Gamma}[2N-m] \quad \text{with} \quad \overline{Z\Gamma}[m] = \hat{C}^*[m]Z\Gamma[m] \tag{4.21}$$

The estimated/equalized version $\hat{q}_{eq}[m]$ of the transmitted information symbol can be attained by utilizing Eq.(4.19), $\hat{C}_c[m]$ and single-tap ZF equalizers. It follows that

$$\hat{q}_{eq}[m] = \frac{\hat{q}[m]}{\hat{C}_c[m]} = J[0]q[m] + \frac{\eta[m]}{\hat{C}_c[m]} \tag{4.22}$$

Substitution of Eq.(4.11) in Eq.(4.22) eventually leads to

$$\hat{q}_{eq}[m] \approx q[m] + j\theta[0]q[m] + \frac{\eta[m]}{\hat{C}_c[m]} \tag{4.23}$$

It is apparent that if $\left|\eta[m]\right| << \left|\hat{C}_c[m]\right|$, then

$$\hat{q}_{eq}[m] \approx q[m] + j\theta[0]q[m] \tag{4.24}$$

Therefore, CPE causes random phase rotation of the desired sample due to $j\theta[0]$. However, when $\theta[0] \to 0$, the estimated transmitted information symbol is found to be

$$\hat{q}_{eq}[m]\Big|_{\theta[0]\to 0} \approx q[m] \tag{4.25}$$

The above scenario is possible subject to the ideal conditions. Practically, in real-time applications, PHN severely deteriorates the performance of F-OFDM system working under fading channels.

4.3. Phase Noise (PHN) Characteristics

In a baseband complex equivalent form [41], the carrier generated by a noisy oscillator may be expressed as

$$f(t) = \exp\{j\phi(t)\} \tag{4.26}$$

where, $\phi(t)$ represents PHN, which is considered to be a continuous-path Brownian motion [56] (or Wiener-Levy process) [34], [39], [57] with zero-mean and variance $2\pi\beta|t|$. Here, the parameter β indicates two-sided 3-dB linewidth of Lorentzian power density spectrum of

oscillator. The PHN can be modelled by using the random-walk paradigm [34], [39], [41], *i.e.*, for $n = 1, 2, \ldots\ldots, N-1$, and it follows that

$$\phi(n) = \phi(n-1) + u(n) \tag{4.27}$$

Here, n indicates the *nth* sample of the OFDM information symbol block with information symbol sampling interval T_s, $u(n)$ is the independent as well as identically distributed (i.i.d.) random variable exhibiting zero-mean and variance $\sigma_u^2 = 2\pi\beta T_s$. Here, $T_s = T/N$ with T indicating duration of one orthogonal frequency division multiplexing information symbol block. Eventually, it is found that $\sigma_u^2 = (2\pi/N)\beta T$ with the PHN rate βT [41]. For the PHN generation through Monte-Carlo simulation, it is assumed that there is perfect phase synchronization at the beginning of OFDM symbol [34], [58], which leads to $\phi(-1) = 0$ (initial value) in the recursive relation for PHN generation in Eq.(4.27), such that $\phi(0) = u(0)$ [33], [59]. It is noteworthy that when the PHN rate $\beta T \to 0$, then the value of variance $\sigma_u^2 \to 0$. For small value of σ_u [degree] and $N \to$ large, the approximate value of $\theta[0] \to 0$ in Eq.(4.24). However, the statistics of random-walk model are quite different from the first-order Markov model (i.e., first-order autoregressive process [60]).

4.4. Results and Discussion

In this section, we will investigate the impact of phase-noise (PHN) [59] on single-tap equalization for fast–OFDM signals [37] under the generic linear fading channels. For simulation, the number of subcarriers is considered to be $N = 256$, which are modulated by using the binary-phase-shift-keying (BPSK). The zero-padding based guard interval with length 64 is utilized in the underlying F–OFDM system, and the ZF based equalization technique is employed to compensate CIR, in the presence of PHN. It is apparent from Eq.(4.20) that the average impact of spectral nulls is lower. Moreover, the signal-to-noise-ratio (SNR) values at the positive frequencies as well as the negative frequencies are averaged optimally without noise amplification [37]. This computationally efficient technique doesn't sacrifice the net information data-rate. It performs well even under the channels with non-symmetric power spectral densities. For the performance evaluation of F–OFDM system in the presence of PHN, four different multipath fading channel scenarios are considered *i.e.*, TWDP fading [50], Rician fading [26], Rayleigh fading [48], [60] and TWDP fading with opposite specular components [51]. The presented results depicting average BER are based on the ensemble average of 250 independent trials (using different channel realizations) at the different values of SNR, which follows that

$$Avg\{BER\}\big|_{SNR} = E\{BER\}\big|_{SNR} \simeq \sum_{a=1}^{250} BER(a)\big|_{SNR} \big/ 250 \tag{4.28}$$

4.4.1. *Case 1*

In this case, we compare the average BER performance of underlying F–OFDM system at the different values of SNR under different fading conditions, in the presence of phase noise. The BER results are demonstrated in Fig. 4.2–Fig. 4.4 at the different values of PHN parameter σ_u^2 i.e., 0.075, 0.1 and 0.125 respectively. At $\sigma_u^2 = 0.075$ (in Fig. 4.2) and $BER = 10^{-4}$, the presence of PHN under TWDP multipath fading conditions causes approximately $2.2dB$ performance loss in terms of SNR. However, this performance loss is observed to be approximately $1.75dB$ in case of the Rician fading channel.

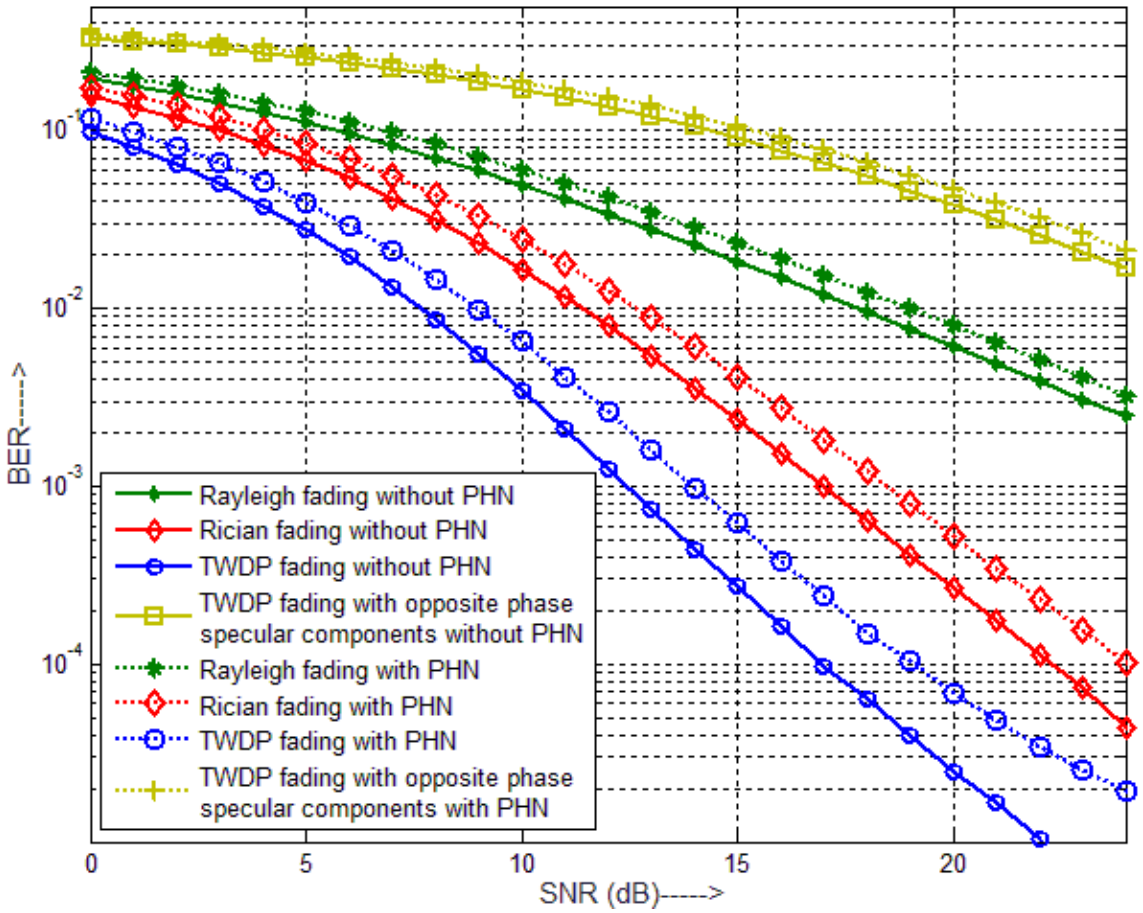

Fig. 4.2. Average BER vs. SNR (dB) with PHN parameter $\sigma_u^2 = 0.075$.

TABLE 4.1. BER AT SNR=+10 dB AND σ_u^2=0.075.

Fading Channel	Rayleigh Fading without PHN	Rayleigh Fading with PHN	Rician Fading without PHN	Rician Fading with PHN	TWDP Fading without PHN	TWDP Fading with PHN
Average BER (approximate values)	4.95×10^{-2}	6.04×10^{-2}	1.65×10^{-2}	2.45×10^{-2}	3.40×10^{-3}	6.50×10^{-3}

TABLE 4.2. BER AT SNR=+20 dB AND σ_u^2=0.075.

Fading Channel	Rayleigh Fading without PHN	Rayleigh Fading with PHN	Rician Fading without PHN	Rician Fading with PHN	TWDP Fading without PHN	TWDP Fading with PHN
Average BER (approximate values)	6.10×10^{-3}	8.0×10^{-3}	2.69×10^{-4}	5.19×10^{-4}	2.50×10^{-5}	6.83×10^{-5}

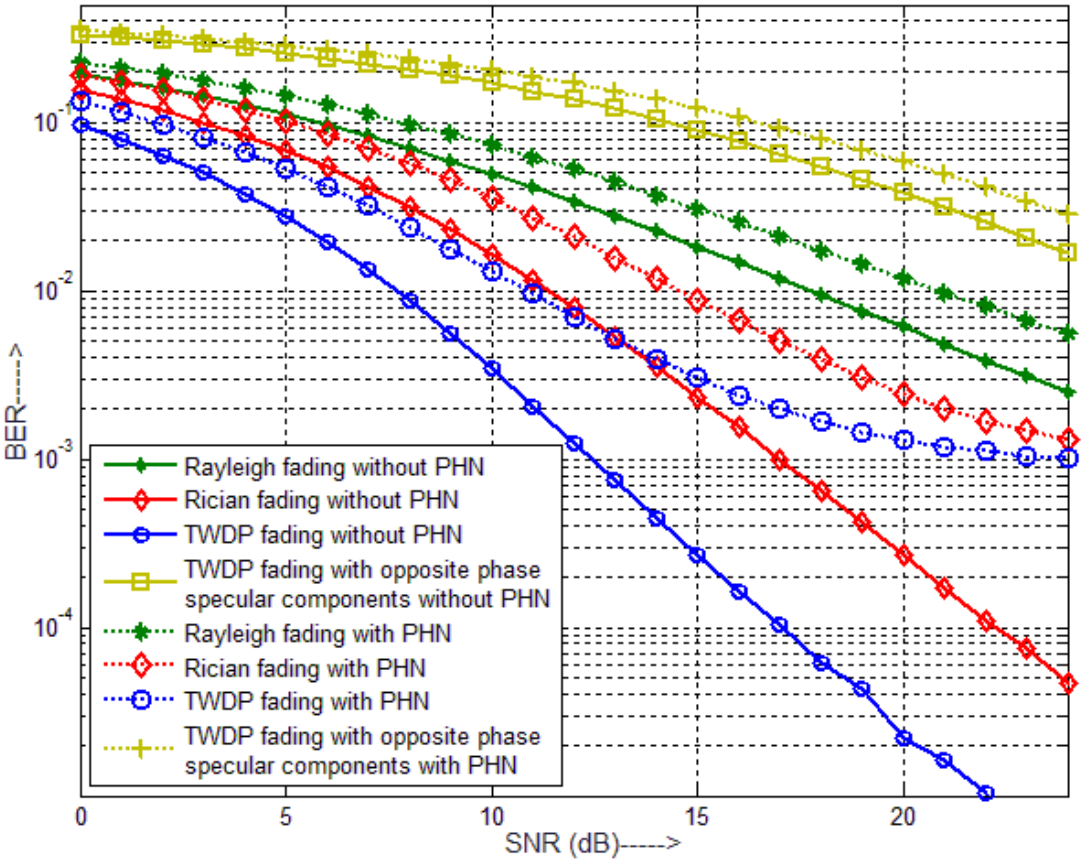

Fig. 4.3. Average BER vs. SNR (dB) with PHN parameter $\sigma_u^2 = 0.1$.

TABLE 4.3. BER AT SNR=+10 dB AND σ_u^2=0.10.

Fading Channel	Rayleigh Fading without PHN	Rayleigh Fading with PHN	Rician Fading without PHN	Rician Fading with PHN	TWDP Fading without PHN	TWDP Fading with PHN
Average BER (approximate values)	4.95×10^{-2}	7.29×10^{-2}	1.65×10^{-2}	3.56×10^{-2}	3.50×10^{-3}	1.31×10^{-2}

TABLE 4.4. BER AT SNR=+20 dB AND σ_u^2=0.10.

Fading Channel	Rayleigh Fading without PHN	Rayleigh Fading with PHN	Rician Fading without PHN	Rician Fading with PHN	TWDP Fading without PHN	TWDP Fading with PHN
Average BER (approximate values)	6.10×10^{-3}	1.18×10^{-2}	2.69×10^{-4}	2.40×10^{-3}	2.20×10^{-5}	1.30×10^{-3}

At $+20dB$ SNR (as shown in Fig. 4.3 and Table 4.4), the average BER is approximately $BER = 2.2\times10^{-5}$ for TWDP fading channel without PHN. But, the BER increases to approximately 0.0013 with PHN parameter $\sigma_u^2 = 0.1$. In case of Rician fading (Fig. 4.3 and Table 4.4), the average BER is approximately 2.69×10^{-4} without PHN, and it is approximately 0.0024 in the presence of similar PHN scenario. However for Rayleigh fading channel, the average BER is approximately 0.0061 without PHN, and the BER is found to be approximately 0.0118 with PHN parameter $\sigma_u^2 = 0.1$, as shown in Fig. 4.3 and Table 4.4.

At $+10dB$ SNR (as shown in Fig. 4.3 and Table 4.3), the average BER is approximately $BER = 3.50\times10^{-3}$ for TWDP fading channel without PHN. But, the BER increases to approximately 0.0131 with PHN parameter $\sigma_u^2 = 0.1$. In case of Rician fading (Fig. 4.3 and Table 4.3), the average BER is approximately 1.65×10^{-2} without PHN, and it is approximately 0.0356 in the presence of similar PHN scenario. However for Rayleigh fading channel, the average BER is approximately 0.0495 without PHN, and the BER is found to be approximately 0.0729 with PHN parameter $\sigma_u^2 = 0.1$, as shown in Fig. 4.3 and Table 4.3.

From results presented in Tables 4.1-4.4, it may be concluded that the approximate average value of BER reduces with the increasing value of SNR. However, the results for TWDP fading in the presence of PHN clearly indicate that its BER performance is better in comparison to the BER performance in case of Rician and Rayleigh fading under similar conditions. Overall, when the value of parameter σ_u^2 increases, the average value of BER gets boosted. Moreover, it is quite clear from Fig. 4.3 that the opposite phase specular components in the TWDP fading signal causes destructive interference in multipath components, which results in high average value of BER irrespective of PHN statistics.

Subsequently, different fading channel conditions/scenarios are considered. At $+20dB$ SNR (as shown in Fig. 4.4 and Table 4.6), the average BER is approximately $BER = 2.61\times10^{-5}$ for TWDP fading channel without PHN. But, the BER increases to approximately 0.0112 with PHN parameter $\sigma_u^2 = 0.125$. In case. of Rician fading as shown in Fig. 4.4 and Table 4.6, the average BER is approximately 2.61×10^{-4} without PHN, and it is approximately 0.0139 in the presence of similar PHN scenario. However for Rayleigh fading channel, the average BER is approximately 0.0061 without PHN, and the BER is found to be approximately 0.0255 with PHN parameter $\sigma_u^2 = 0.125$ as per Fig. 4.4 and Table 4.6.

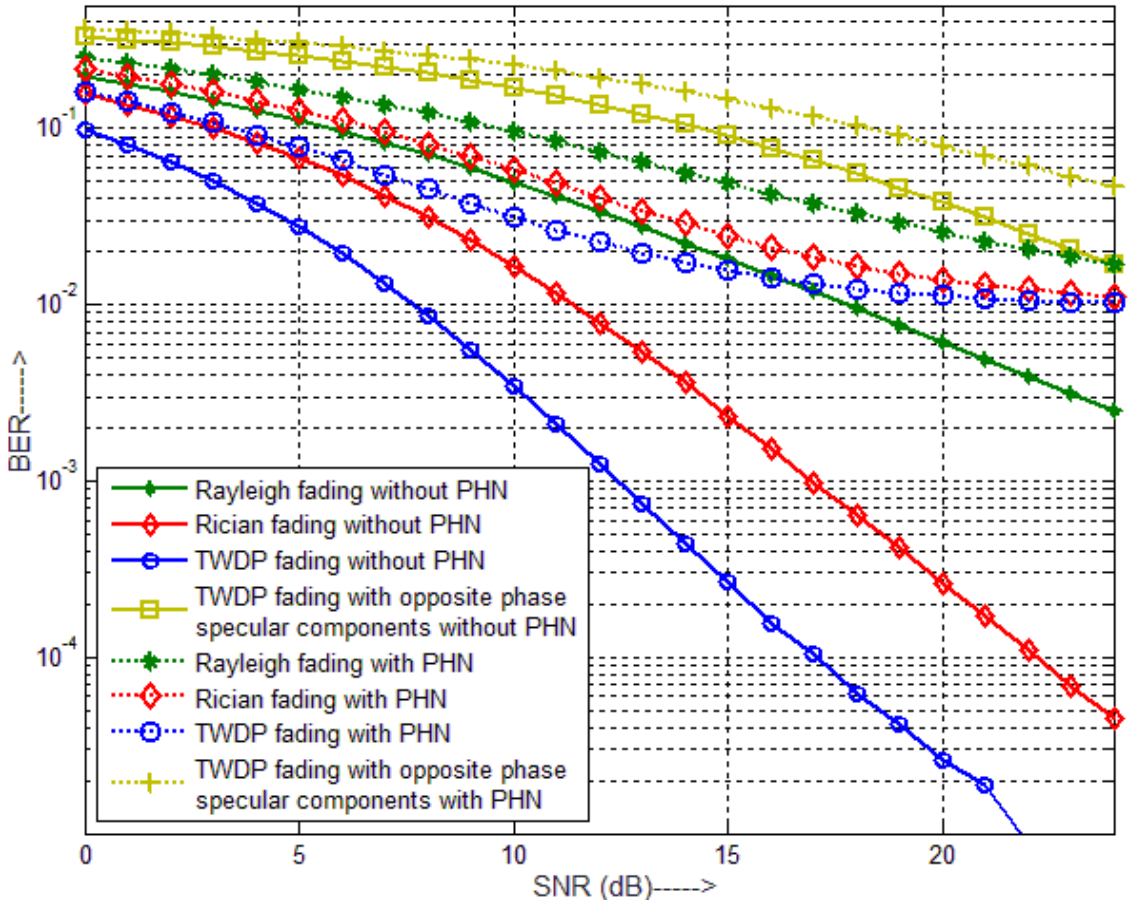

Fig. 4.4. Average BER vs. SNR (dB) with PHN parameter $\sigma_u^2 = 0.125$.

TABLE 4.5. BER AT SNR=+10 dB AND $\sigma_u^2 = 0.125$.

Fading Channel	Rayleigh Fading without PHN	Rayleigh Fading with PHN	Rician Fading without PHN	Rician Fading with PHN	TWDP Fading without PHN	TWDP Fading with PHN
Average BER (approximate values)	4.95×10^{-2}	9.55×10^{-2}	1.66×10^{-2}	5.79×10^{-2}	3.40×10^{-3}	3.14×10^{-2}

TABLE 4.6. BER AT SNR=+20 dB AND $\sigma_u^2 = 0.125$.

Fading Channel	Rayleigh Fading without PHN	Rayleigh Fading with PHN	Rician Fading without PHN	Rician Fading with PHN	TWDP Fading without PHN	TWDP Fading with PHN
Average BER (approximate values)	6.10×10^{-3}	2.550×10^{-2}	2.6135×10^{-4}	1.390×10^{-2}	2.61×10^{-5}	1.120×10^{-2}

At $+10dB$ SNR (as shown in Fig. 4.4 and Table 4.5), the average BER is approximately $BER = 3.40 \times 10^{-3}$ for TWDP fading channel without PHN. But, the BER increases to approximately 0.0314 with PHN parameter $\sigma_u^2 = 0.125$. In case of Rician fading as shown in Fig. 4.4 and Table 4.5, the average BER is approximately 1.66×10^{-2} without PHN, and it is approximately 0.0579 in the presence of similar PHN scenario. However for Rayleigh fading channel, the average BER is approximately 0.0495 without PHN, and the BER is found to be approximately 0.0955 with PHN parameter $\sigma_u^2 = 0.125$ as per Fig. 4.4 and Table 4.5.

It is apparent from the simulation results depicted in Fig. 4.2–Fig. 4.4 that the BER performance of F–OFDM system gets deteriorated severely for the typical case of TWDP fading with opposite phase specular components without PHN (worst case scenario). However, the presence of PHN further degrades the BER performance of underlying F–OFDM system. This degradation substantially increases with the elevating value of PHN parameter σ_u^2. However, the lowest BER values are observed in case of TWDP multipath fading channel. Based on the simulation trials, it is clear that BER(TWDP channel) < BER(Rician channel) < BER(Rayleigh channel).

4.4.2. *Case 2*

In this case, we compare the average BER performance of underlying F–OFDM system at the different values of PHN parameter σ_u^2 in Eq.(4.27), under different fading conditions, while keeping the SNR value fixed. The BER results are depicted in Fig. 4.5–Fig. 4.8 and Tables 4.7-4.17 at the different values of SNR i.e., +10dB, +15dB, +20dB and +25dB respectively.

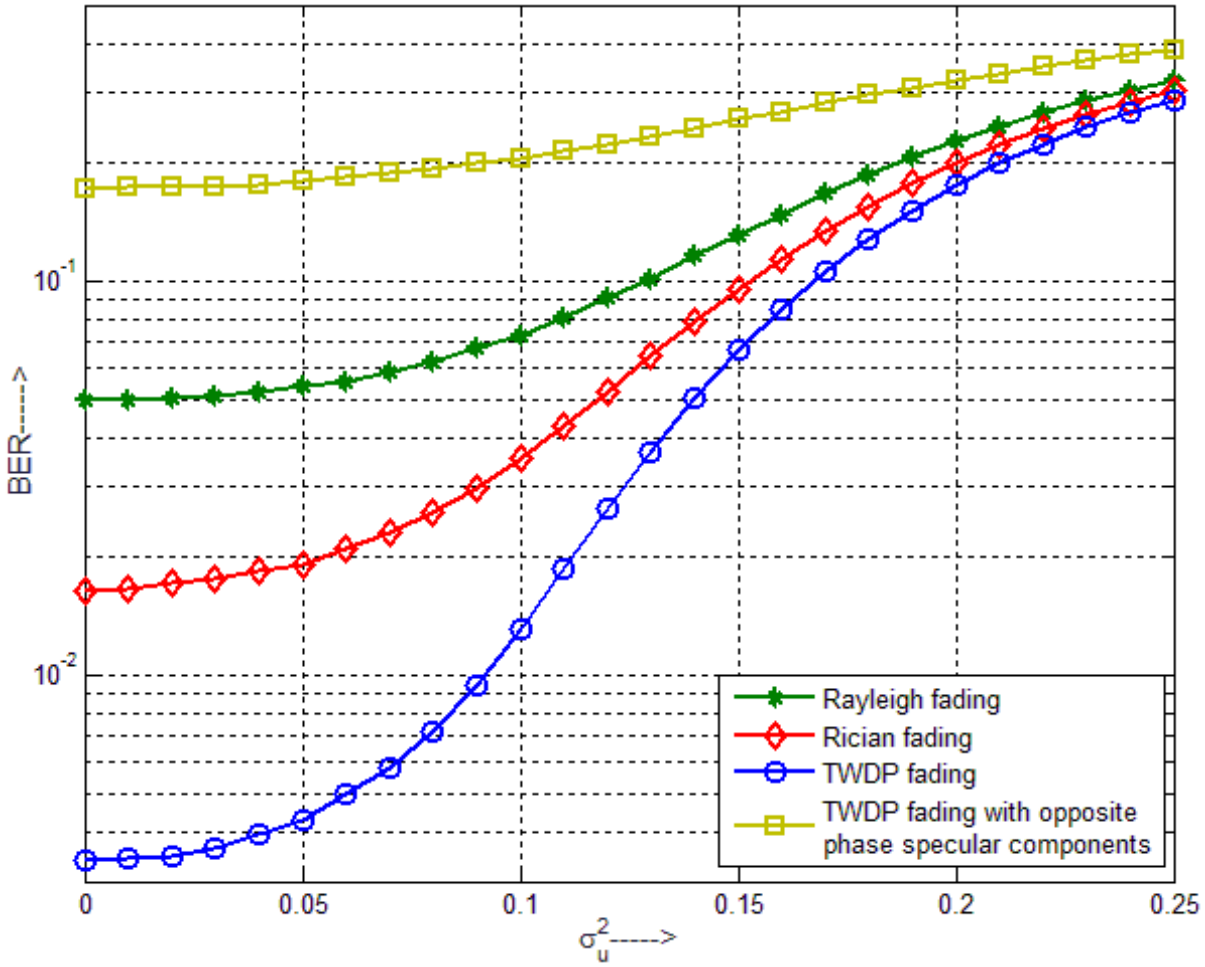

Fig. 4.5. Average BER vs. PHN parameter σ_u^2 at SNR = +10dB.

TABLE 4.7. BER AT SNR=+10 dB AND σ_u^2=0.05.

Fading Channel	Rayleigh Fading with PHN	Rician Fading with PHN	TWDP Fading with PHN	TWDP with opposite phase specular components with PHN
Average BER (approximate values)	5.42×10^{-2}	1.91×10^{-2}	4.30×10^{-3}	1.79×10^{-1}

TABLE 4.8. BER AT SNR=+10 dB AND σ_u^2=0.10.

Fading Channel	Rayleigh Fading with PHN	Rician Fading with PHN	TWDP Fading with PHN	TWDP with opposite phase specular components with PHN
Average BER (approximate values)	7.22×10^{-2}	3.55×10^{-2}	1.30×10^{-2}	2.05×10^{-1}

TABLE 4.9. BER AT SNR=+10 dB AND σ_u^2 =0.15.

Fading Channel	Rayleigh Fading with PHN	Rician Fading with PHN	TWDP Fading with PHN	TWDP with opposite phase specular components with PHN
Average BER (approximate values)	1.31×10^{-1}	9.50×10^{-2}	6.67×10^{-2}	2.56×10^{-1}

At $SNR=+15dB$ and $\sigma_u^2=0.05$, the simulation results demonstrated in Fig. 4.6 and Table 4.10 indicate that the approximate value of average $BER=3.5\times10^{-4}$ for TWDP fading channel, $BER=2.7\times10^{-3}$ for Rician fading, $BER=0.02$ for Rayleigh fading channel. However, the BER is observed to be 0.1 for the typical case of TWDP fading with opposite phase specular components (worst case scenario). Further at $SNR=+25dB$ and $\sigma_u^2=0.05$, the simulation results presented in Fig. 4.8 and Table 4.16 illustrate that the average $BER=3.2\times10^{-6}$ for TWDP fading channel, $BER=3.4\times10^{-5}$ for Rician fading, $BER=2.2\times10^{-3}$ for Rayleigh fading channel. However, the BER is observed to be 0.015 for the typical case of TWDP fading with opposite phase specular components (worst case).

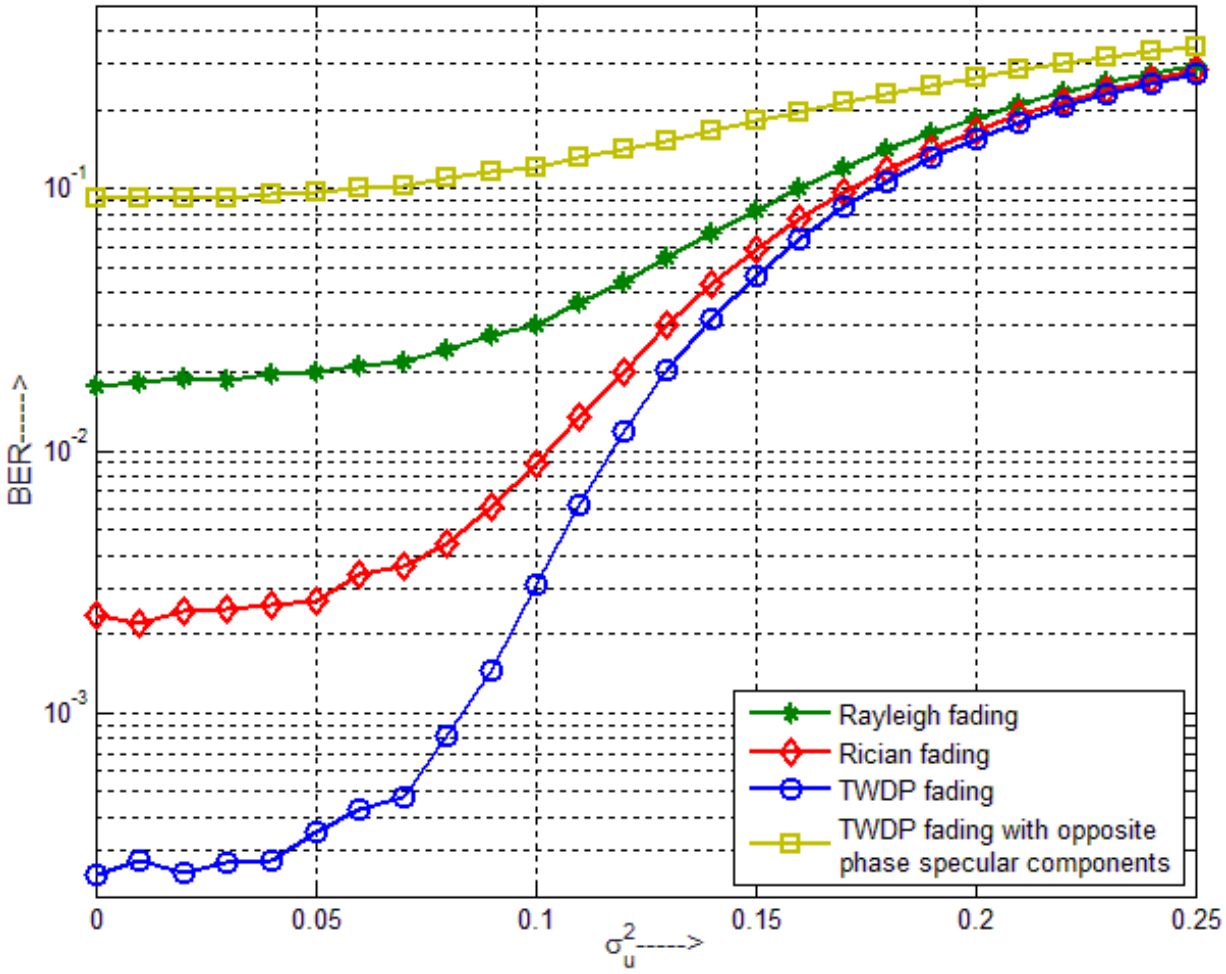

Fig. 4.6. Average BER vs. PHN parameter σ_u^2 at SNR = +15dB.

TABLE 4.10. BER AT SNR=+15 dB AND σ_u^2=0.05.

Fading Channel	Rayleigh Fading with PHN	Rician Fading with PHN	TWDP Fading with PHN	TWDP with opposite phase specular components with PHN
Average BER (approximate values)	2.0×10^{-2}	2.70×10^{-3}	3.5×10^{-4}	0.1

TABLE 4.11. BER AT SNR=+15 dB AND σ_u^2=0.10

Fading Channel	Rayleigh Fading with PHN	Rician Fading with PHN	TWDP Fading with PHN	TWDP with opposite phase specular components with PHN
Average BER (approximate values)	3.03×10^{-2}	8.90×10^{-3}	3.10×10^{-3}	1.208×10^{-1}

TABLE 4.12. BER AT SNR=+15 dB AND σ_u^2=0.15.

Fading Channel	Rayleigh Fading with PHN	Rician Fading with PHN	TWDP Fading with PHN	TWDP with opposite phase specular components with PHN
Average BER (approximate values)	8.26×10^{-2}	5.83×10^{-2}	4.67×10^{-2}	1.79×10^{-1}

At $SNR=+15dB$ and $\sigma_u^2=0.15$, the simulation results demonstrated in Fig. 4.6 and Table 4.12 indicate that the approximate value of average $BER=4.67\times10^{-2}$ for TWDP fading channel, $BER=5.83\times10^{-2}$ for Rician fading, $BER=0.0826$ for Rayleigh fading channel. However, the BER is observed to be 0.179 for the typical case of TWDP fading with opposite phase specular components (worst case scenario). Further at $SNR=+25dB$ and $\sigma_u^2=0.1$, the simulation results presented in Fig. 4.8 and Table 4.17 illustrate that the average $BER=9.755\times10^{-4}$ for TWDP fading channel, $BER=1.2\times10^{-3}$ for Rician fading, $BER=4.6\times10^{-3}$ for Rayleigh fading channel. However, the BER is observed to be 0.0235 for the typical case of TWDP fading with opposite phase specular components (worst case).

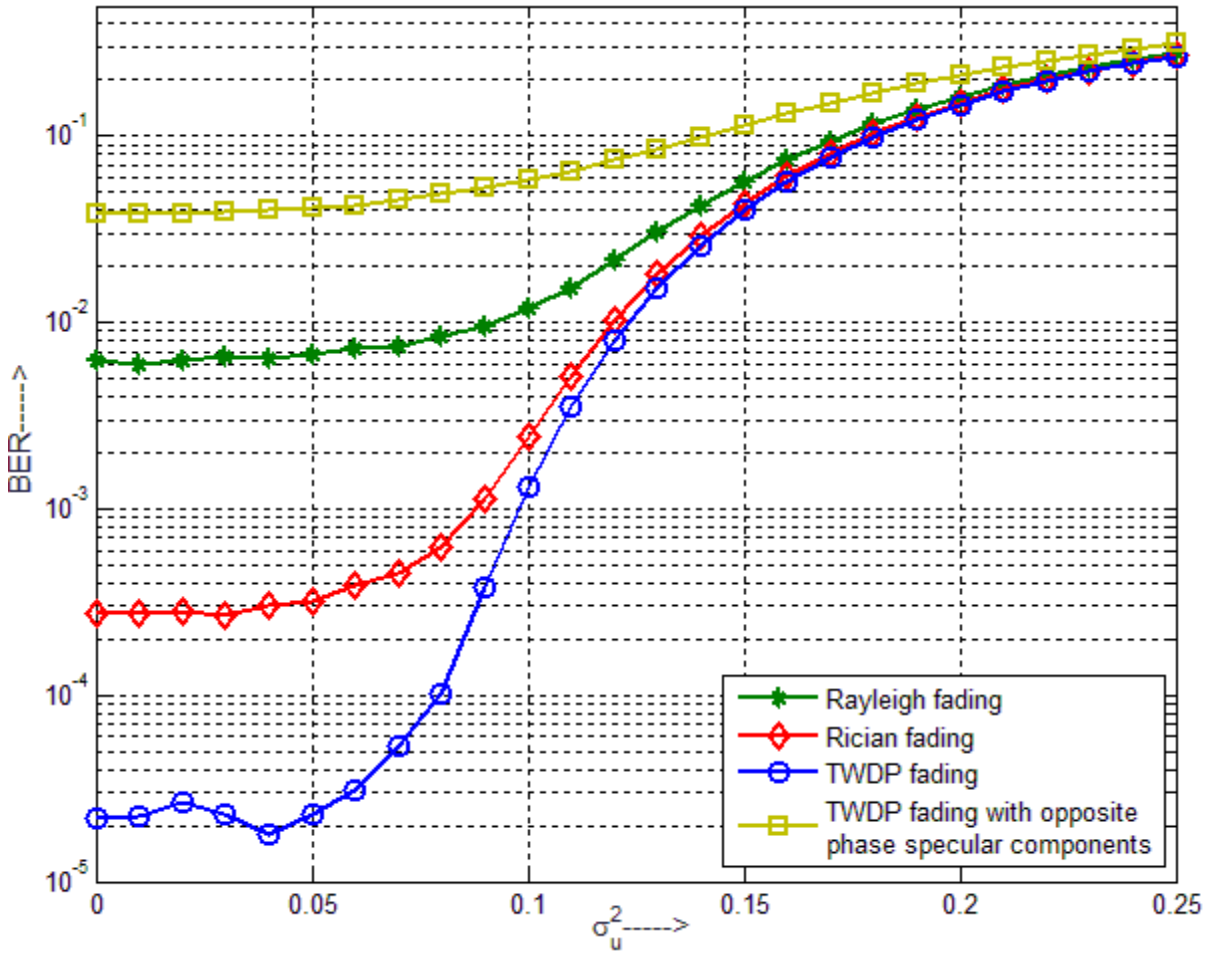

Fig. 4.7. Average BER vs. PHN parameter σ_u^2 at SNR = +20dB.

TABLE 4.13. BER AT SNR=+20 dB AND σ_u^2=0.05.

Fading Channel	Rayleigh Fading with PHN	Rician Fading with PHN	TWDP Fading with PHN	TWDP with opposite phase specular components with PHN
Average BER (approximate values)	6.80×10^{-3}	3.17×10^{-4}	2.28×10^{-5}	4.18×10^{-2}

TABLE 4.14. BER AT SNR=+20 dB AND σ_u^2=0.10.

Fading Channel	Rayleigh Fading with PHN	Rician Fading with PHN	TWDP Fading with PHN	TWDP with opposite phase specular components with PHN
Average BER (approximate values)	1.20×10^{-2}	2.40×10^{-3}	1.30×10^{-3}	5.81×10^{-2}

TABLE 4.15. BER AT SNR=+20 dB AND σ_u^2=0.15.

Fading Channel	Rayleigh Fading with PHN	Rician Fading with PHN	TWDP Fading with PHN	TWDP with opposite phase specular components with PHN
Average BER (approximate values)	5.690×10^{-2}	4.380×10^{-2}	3.990×10^{-2}	1.147×10^{-1}

It is clear from results shown in Fig. 4.5 – Fig. 4.8 and Tables 4.7-4.17 that the phase noise adversely affects the BER performance of F – OFDM system, as the value of PHN parameter σ_u^2 increases. Moreover, the elevating value of SNR leads to significant reduction in the average BER under all fading scenarios.

4.4.3. *Case 3*

In this case, we compare the average BER performance of underlying F-OFDM system at the different values of SNR under different fading conditions, in the presence of phase noise exhibiting low and high values of variance. At low value of PHN parameter σ_u^2=0.05 and SNR=+10dB, the average value of BER for TWDP fading without PHN is 3.50×10^{-3}, and it is 5.0×10^{-3} in the presence of PHN (as indicated in Fig. 4.9 and Table 4.18). At SNR=+20dB and σ_u^2=0.05, the average value of BER for TWDP fading without PHN is 2.55×10^{-5} and it is 3.45×10^{-5} in the presence of PHN (as indicated in Fig. 4.9 and Table 4.19). It is observed that the performance degradation in terms of SNR is less than +1dB when $\sigma_u^2 \le 0.05$. Therefore, for low values of PHN parameter σ_u^2, the BER performance degradation of F-OFDM system is marginal.

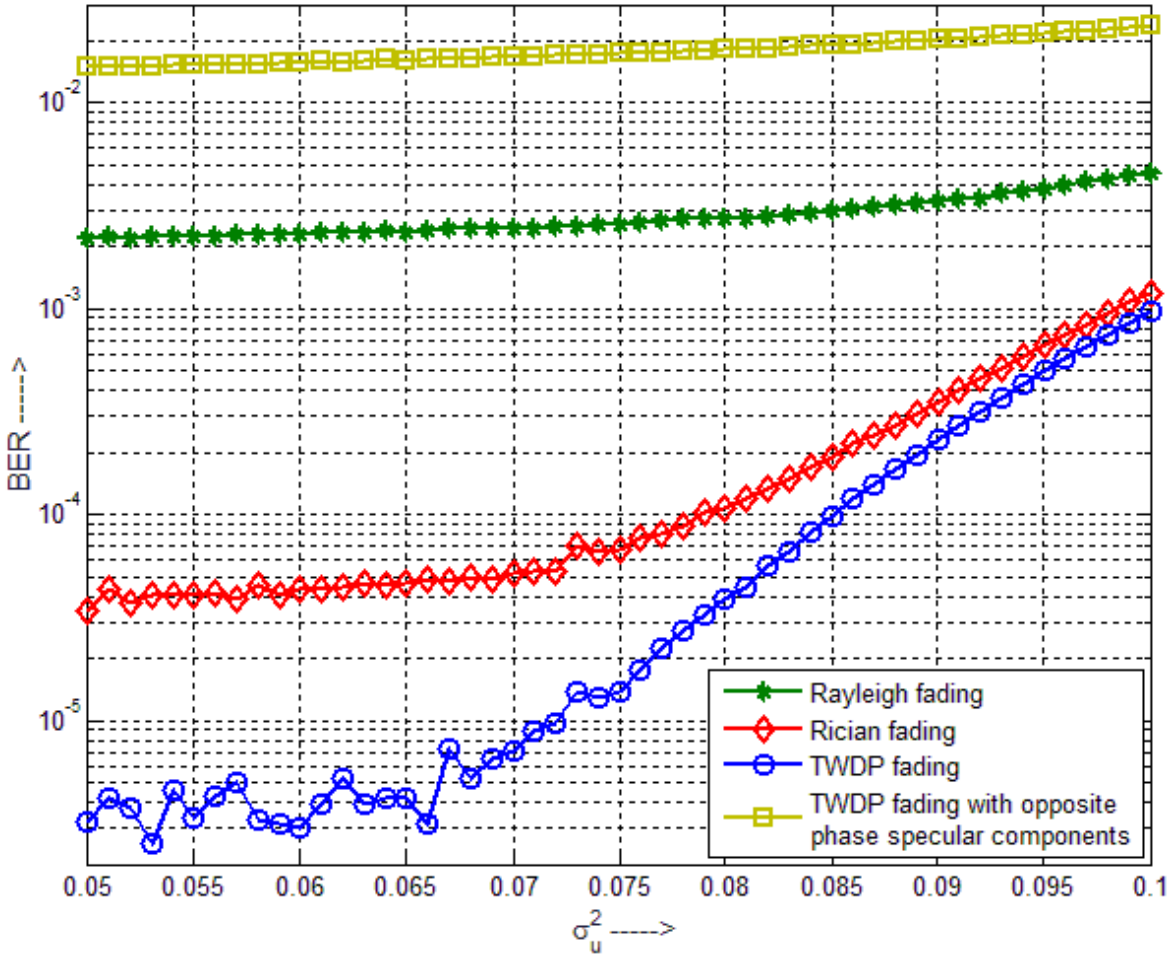

Fig. 4.8. Average BER vs. PHN parameter σ_u^2 at SNR = +25dB.

TABLE 4.16. BER AT SNR=+25 dB AND σ_u^2=0.05.

Fading Channel	Rayleigh Fading with PHN	Rician Fading with PHN	TWDP Fading with PHN	TWDP with opposite phase specular components with PHN
Average BER (approximate values)	2.20×10^{-3}	3.4×10^{-5}	3.2×10^{-6}	0.015

TABLE 4.17. BER AT SNR=+25 dB AND σ_u^2=0.10.

Fading Channel	Rayleigh Fading with PHN	Rician Fading with PHN	TWDP Fading with PHN	TWDP with opposite phase specular components with PHN
Average BER (approximate values)	4.60×10^{-3}	1.20×10^{-3}	9.755×10^{-4}	2.350×10^{-2}

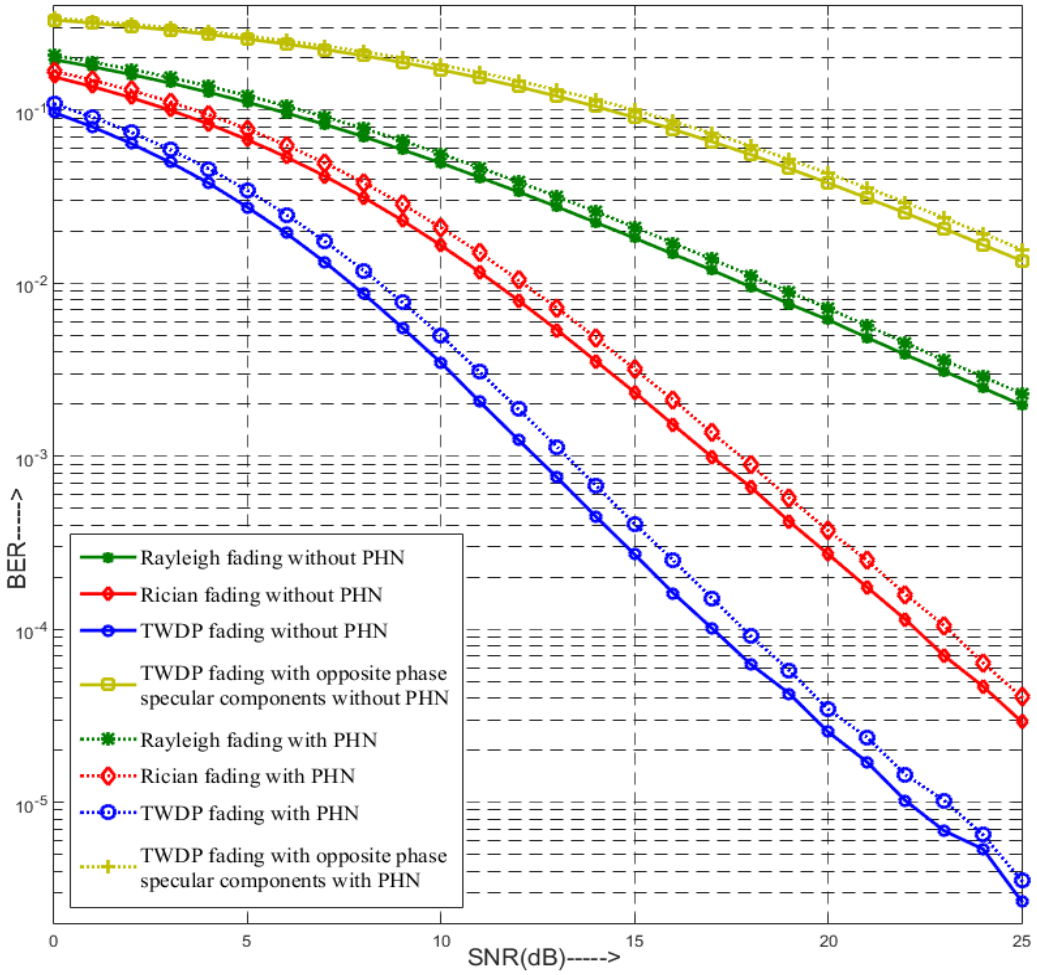

Fig. 4.9. Average BER vs. SNR (dB) with PHN parameter σ_u^2=0.05.

TABLE 4.18. BER AT SNR=+10 dB AND σ_u^2=0.05.

Fading Channel	Rayleigh Fading without PHN	Rayleigh Fading with PHN	Rician Fading without PHN	Rician Fading with PHN	TWDP Fading without PHN	TWDP Fading with PHN
Average BER (approximate values)	4.95×10^{-2}	5.06×10^{-2}	1.65×10^{-2}	2.09×10^{-2}	3.50×10^{-3}	5.0×10^{-3}

TABLE 4.19. BER AT SNR=+20 dB AND σ_u^2=0.05.

Fading Channel	Rayleigh Fading without PHN	Rayleigh Fading with PHN	Rician Fading without PHN	Rician Fading with PHN	TWDP Fading without PHN	TWDP Fading with PHN
Average BER (approximate values)	6.10×10^{-3}	7.20×10^{-3}	2.72×10^{-4}	3.72×10^{-4}	2.55×10^{-5}	3.45×10^{-5}

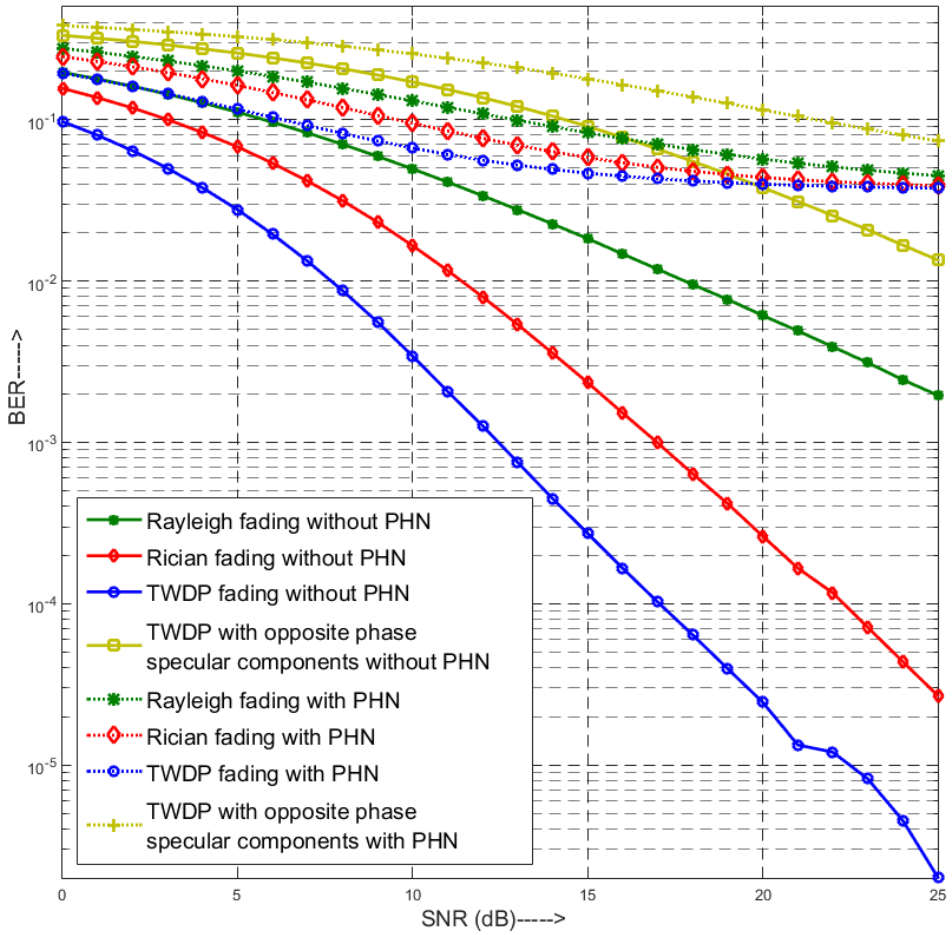

Fig. 4.10. Average BER vs. SNR (dB) with PHN parameter σ_u^2=0.15.

TABLE 4.20. BER AT SNR=+10 dB AND σ_u^2=0.15.

Fading Channel	Rayleigh Fading without PHN	Rayleigh Fading with PHN	Rician Fading without PHN	Rician Fading with PHN	TWDP Fading without PHN	TWDP Fading with PHN
Average BER (approximate values)	4.95×10^{-2}	1.31×10^{-1}	1.66×10^{-2}	9.50×10^{-2}	3.40×10^{-3}	6.67×10^{-2}

TABLE 4.21. BER AT SNR=+20 dB AND σ_u^2=0.15.

Fading Channel	Rayleigh Fading without PHN	Rayleigh Fading with PHN	Rician Fading without PHN	Rician Fading with PHN	TWDP Fading without PHN	TWDP Fading with PHN
Average BER (approximate values)	6.10×10^{-3}	5.69×10^{-2}	2.62×10^{-4}	4.38×10^{-2}	2.45×10^{-5}	3.98×10^{-2}

At high value of PHN parameter σ_u^2=0.15 and SNR=+10dB, the average value of BER for TWDP fading without PHN is 3.40×10^{-3}, and it is 6.67×10^{-2} in the presence of PHN (as indicated in Fig. 4.10 and Table 4.20). At SNR=+20dB and σ_u^2=0.15, the average value of BER for TWDP fading without PHN is 2.45×10^{-5}, and it is 3.98×10^{-2} in the presence of PHN (as indicated in Fig. 4.10 and Table 4.21). It is clear from research outcomes demonstrated in Fig. 4.10 and Table 4.20 - Table 4.21 that a drastic degradation in BER performance of F-OFDM system comes into picture due to presence of PHN (at high values of PHN parameter σ_u^2) under all types of fading conditions. Under this situation the increasing value of SNR can only control the BER degradation to some extent.

4.5. Summary of Chapter

This chapter has addressed the impact of phase noise on the single-tap zero-forcing equalization for F-OFDM signals, while working under the generic multipath fading channels. We have compared the average BER performance results for F–OFDM system in the presence of PHN as well as in the absence of PHN. The phase noise samples are assumed to follow Brownian motion using the random-walk model. The underlying F–OFDM system compensates the LTI channel with any symmetric channel constraint on CIR, in the presence of AWGN and PHN. Here, the DCT operation at receiver is replaced by the extended DFT operation for the efficient designing (as in [16]). Three major types of the multipath fading channels are considered for simulation i.e., TWDP, Rician and Rayleigh.

Simulation results connote that the average BER is lowest while working under TWDP fading environment. The BER is observed to be higher in case of Rician and Rayleigh fading environment as compared to the TWDP fading case. However, the bit detection success rate performance under the Rician channel is quite appreciable in comparison to the Rayleigh fading channel case. Moreover, this is concluded from research outcomes that the large PHN variations severely affect the average BER performance of F–OFDM system. As the value of PHN parameter σ_u [degree] gets elevated or the PHN rate rises, the BER increases dramatically. Under typical conditions/case, when two specular components in TWDP fading are equal in strength and opposite in phase at the receiving end, then receiver in F–OFDM system is found to perform worse than the Rayleigh fading case.

Chapter 5

CONCLUDING REMARKS AND FUTURE SCOPE

5.1. Concluding Remarks

In the domain of fiber optic communication systems, the discrete–cosine–transform (DCT) is usually preferred over the discrete–Fourier–transform (DFT) in Fast (F) – OFDM systems for the information symbol multiplexing onto the N subcarriers. Exclusively, F–OFDM possesses enhanced tolerance, to the carrier frequency offset in optical coherent detection, as well as to the Doppler shift in wireless communication. These striking features make the F–OFDM an efficient and suitable technique for multi-carrier (MC) transmission. But, one of the key challenges in communication systems utilizing the DCT based F–OFDM technique is that DCT exhibits symmetric convolution property. Under generic linear fading channel conditions (like modal dispersion in multi-mode-fiber optic channel and multipath fading in wireless channel), the condition for symmetric convolution is not fulfilled, and it precludes the usage of traditional single-tap equalizers for channel-impulse-response (CIR) compensation. Therefore to compensate generic linear-time-invariant (LTI) channels by utilizing a single-tap equalizer without compromising the data-rate, in addition to zero-padded guard interval, the DFT of double length (2N–point) has been incorporated at the receiver instead of the conventional N–point DCT approach. However, the MC modulation possesses a substantial sensitivity to the phase-noise (PHN) of the oscillator utilized for frequency down-conversion at receiver. The PHN disturbs the orthogonality of OFDM subcarriers, and it results both in rotation of every subcarrier by a random phase, called common-phase-error, and to inter-carrier-interference (ICI). However, the higher PHN levels are catastrophic, as it makes ICI dominant over the transmitted signal.

The underlying F–OFDM system compensates the LTI channel with any symmetric channel constraint on CIR, in the presence of AWGN and PHN. The simulation results connote that the average BER is lowest while working under TWDP fading channel. The BER is observed to be higher in case of Rician and Rayleigh fading as compared to the TWDP fading case. However, the bit detection success rate performance under Rician channel is quite appreciable in comparison to the Rayleigh fading channel case. Moreover, it is concluded from research outcomes that the large PHN variations severely affect the BER performance of F–OFDM

system. As the value of PHN rate gets elevated, the BER increases dramatically. Under typical conditions, when two specular components in TWDP fading are equal in strength as well as opposite in phase at receiving end, then F–OFDM system is found to perform worse than the Rayleigh fading case. This inference points towards the utilization of TWDP fading rather than Rayleigh fading as a worst case scenario in evaluating the communication systems, and these results are in close agreement with the recent studies in this field.

5.2. Future Scope

Future work includes the investigation of BER performance of aforementioned F–OFDM system in the presence of impulse noise in addition to the PHN and AWGN [61], [62]. The detrimental effects of PHN on the performance of F–OFDM systems need to be compensated/mitigated through the application of adaptive and blind techniques [33], [52]. In the presented research work, the perfect CSI is considered to be available at the receiver. However, the communication system performance ought to be explored, when only imperfect CSI [61]-[62] is available at receiver.

REFERENCES

[1] M. Alard and R. Lasalle, “Principles of modulation and channel coding for digital broadcasting for mobile receivers,” *EBY Rev.*, vol. 224, pp. 47-69, Aug. 1987.

[2] J. A. C. Bingam, “Multicarrier modulation for data transmission: An idea whose time has come,” *IEEE Commun. Mag.*, vol. 28, no. 1, pp. 5-14, May 1990.

[3] L. J. Cimini Jr., “Analysis and simulation of a digital mobile channel using orthogonal frequency division multiplexing,” *IEEE Trans. Commun.*, vol. 33, no. 7,pp. 665-675, Jul. 1985.

[4] J. Armstrong, “OFDM for optical communications,” *IEEE J. Lightw. Technol.*, vol. 27, no. 3, pp. 189-204, Feb. 2009.

[5] Y. Li and L. J. Cimini, “Bounds on the interchannel interference of OFDM in time-varying impairments,” *IEEE Trans. Commun.*, vol. 49, no. 3, pp. 401-404, Mar. 2001.

[6] A. Zainudin, A. Sudarsono, and I. G. P. Astawa, “Performance analysis of an OFDM scheme with zero forcing equalizer using software defined radio platform and USRP,” *EMITTER Int. J. Engg. Technol.*, vol. 2, no. 1, Jun. 2014.

[7] T. Rappaport, *Wireless Communications: Principles and Practice*, 2nd ed. Englewood Cliffs, New Jersey: Prentice-Hall, 1996.

[8] K. Sathananthan and C. Tellambura, "Probability of error calculation of OFDM systems with frequency offset," *IEEE Trans. Commun.*, vol. 49, no. 11, pp. 1884-1888, Nov. 2001.

[9] L. Wan and V. K. Dubey, "BER performance of OFDM system over frequency nonselective fast Ricean fading channels," *IEEE Commun. Lett.*, vol. 5, no. 1, pp. 19-21, Jan. 2001.

[10] M. Rodrigues and I. Darwazeh, “Fast OFDM: A proposal for doubling the data rate of OFDM schemes,” in *Proc. IEEE ICT*, Beijing, China, 2002, pp. 484-487.

[11] W. Long, J. Zhang, D. Wang, J. Han, S. Chen, A. M. Han, G. Gao, H. Leng, W. Zhu, Y. Zhao, and W. Gu, “Mitigation of the interference between odd and even terms in optical fast OFDM scheme based on interleaved multiplexting,” *IEEE Photon. Technol. Lett.*, vol. 24, no. 13, pp. 1160-1162, Jul. 2012.

[12] X. Ouyang, J. Jin, G. Jin, Z. Wang, and Y. Park, "Interleaved multiplexing optical fast OFDM without the interference between subchannels," *IEEE Photon. Technol. Lett.*, vol. 25, no. 4, pp. 378-381, Feb. 2013.

[13] F. Xiong, "M-ary amplitude shift keying OFDM system," *IEEE Trans. Commun.*, vol. 51, no. 10, Oct. 2003.

[14] J. Zhao and H. Shams, "Fast dispersion estimation in coherent optical 16QAM fast OFDM systems," *Opt. Exp.*, vol. 21, no. 2, pp. 2500-2505, Jan. 2013.

[15] E. Giacoumids, S. K. Ibrahim, J.Zhao, J.M. Tang, A.D. Ellis, and I. Tomokos, "Experimental and theoretical investigations of intensity-modulation and direct-detection optical fast-OFDM over MMF-links," *IEEE Photon. Technol. Lett.*, vol. 24, no. 1, pp. 52-54, Jan. 2012.

[16] P. Tan and N. C. Beaulieu, "A comparison of DCT-based OFDM and DFT-based OFDM in frequency offset and fading channels," *IEEE Trans. Commun.*, vol. 54, no. 11, pp. 2113-2115, Nov. 2006.

[17] J. Zhao and A. Ellis, "Advantage of Optical fast OFDM over OFDM in residual frequency offset compensation," *IEEE Photon. Technol. Lett.*, vol. 24, no. 24, pp. 2284-2287, Dec. 2012.

[18] J. Zhao, "Intensity-modulation full-field detection optical fast OFDM," *J. Opt. Commun. Netw.*, vol 5, no. 5, pp. 465-474, May 2013.

[19] S. A. Martucci, "Symmetric convolution and discrete sine and cosine transforms," *IEEE Trans. Signal Process.*, vol. 42, no. 5, pp. 1038-1051, May 1994.

[20] J. Zhao and A. Ellis, "Transmission of 4-ASK optical fast OFDM with chromatic dispersion compensation," *IEEE Photon Technol. Lett.*, vol. 24, no. 1, pp. 34-36, Jan. 2012.

[21] G. D. Mandyam, "Sinusoidal transforms in OFDM systems," *IEEE Trans. Broadcast.*, vol. 50, no. 2, pp. 172-184, Jun. 2004.

[22] N. Al-Dhahir, H Minn, and S. Satish, "Optimum DCT-based multicarrier transceivers for frequency-selective channels," *IEEE Trans. Commun.*, vol. 54, no. 5, pp. 911-921, May 2006.

[23] D. Falconer, S. L. Ariyavisitakul, A. Benyamin-Seeyar, and B. Eidson, "Frequency domain equalization for single-carrier broadband wireless systems," *IEEE Commun. Mag.*, vol. 40, no. 4, pp. 54-66, Apr. 2002.

[24] F. Cruz-Roldan, M. E. Dominguez-Jimenez, G. S. Vidal, P. Amo-Lopez, M. Blanco-Velasco, and A. Bravo-Santos, "On the use of discrete cosine transform for multicarrier communications," *IEEE Trans. Signal Process.*, vol. 60, no. 11, Nov. 2012.

[25] A.V. Oppenheim, *Discrete Time Signal Processing*, 2nd ed. Upper Saddle River, New Jersey: Prentice-Hall, 1998.

[26] G. D. Durgin, T. S. Rappaport, and D. A. de Wolf, "New analytical models and probability density functions for fading in wireless communication," *IEEE Trans. Wireless Commun.*, vol. 50, no. 6, pp. 1005-1015, Jun. 2002.

[27] F. Gao, T. Cui, A. Nallanathan, and C. Tellambura, "Maximum likelihood based estimation of frequency and phase offset in DCT OFDM systems under non-circular transmissions: Algorithms, analysis and comparisons," *IEEE Trans. Commun.*, vol. 56, no. 9, pp. 1425–1429, Sep. 2008.

[28] V. Sánchez, P. García, A. M. Peinado, J. C. Segura, and A. J. Rubio, "Diagonalizing properties of the discrete cosine transforms," *IEEE Trans. Signal Process.*, vol. 43, no. 11, pp. 2631–2641, Nov. 1995.

[29] C. He, L. Zhang, J. Mao, A. Cao, P. Xiao, and M. A. Imran, "Performance analysis and optimization of DCT-based multicarrier system on frequency-selective fading channels," *IEEE Access*, Published Online 2018.

[30] T. Rappaport, *Wireless Communication, Principles and Practice*, 2nd ed. Englewood Cliffs, NJ: Prentice-Hall, 2002.

[31] H. Zen, "Performance evaluation of 2-D pilot aided OFDM system under hiper Rayleigh fading channel," *The University of Toledo, M.Sc. Thesis*, 2011.

[32] S. H. Oh, K. H. Li, and W. S. Lee, "Performance of BPSK pre-detection MRC systems over two-wave with diffuse power fading channels," *IEEE Trans Wireless Commun.*, vol. 6, no. 8, pp. 2772-2775, Aug. 2007.

[33] S. Wu and Y. Bar-Ness, "A phase noise suppression algorithm for OFDM-based WLANs," *IEEE Commun. Lett.*, vol. 6, no. 12, pp. 535-537, Dec. 2002.

[34] L. Tomba, "On the effect of wiener phase noise in OFDM systems," *IEEE Trans. Commun.*, vol. 46, no. 5, pp. 580-583, May 1998.

[35] M. K. Lee, S. C. Lim, and K. Yang, "Blind compensation for phase noise in OFDM systems over constant modulus modulation," *IEEE Commun.*, vol. 60, no. 3, pp. 620-625, Mar. 2012.

[36] F. Adachi, H. Tomeba, and K. Takeda, "Frequency–domain equalization for broadband single-carrier multiple access," *IEICE Trans. Commun.*, vol. E92-B, no. 5, pp. 1441-1456, May 2009.

[37] X. Ouyang and J. Zhao, "Single-tap equalization for fast OFDM signals under generic linear channels," *IEEE Commun. Lett.*, vol. 18, no. 8, pp. 1319-1322, Aug. 2014.

[38] M. Webster, L. Raddatz, I.H. White, and D. G. Cunninghan, "A statistical analysis of conditioned launch for gigabit Ethernet links using multimode fiber," *IEEE J. Lightw. Technol.*, vol. 17, no. 9, pp. 1532-1541, Sep. 1999.

[39] T. Pollet, M. Van Bladel, and M. Moeneclaey, "BER sensitivity of OFDM systems to carrier frequency offset and wiener phase noise," *IEEE Trans. Commun.*, vol. 43, no. 2, pp. 191-193, Feb. 1995.

[40] C. Garnier, L. Clavier, Y. Delignon, M. Loosvelt, and D. Boulinguez, "Multiple access for 60 GHz mobile ad hoc network," in *Proc. IEEE VTC Spring*, vol. 3, May 2002, pp. 1517-1521.

[41] F. Septier, Y. Delignon, A. Menhaj-Rivenq, and C. Garnier, "Monte carlo methods for channel, phase noise, and frequency offset estimation with unknown noise variances in OFDM systems," *IEEE Trans. Signal Process.*, vol. 56, no. 8, pp. 3613-3626, Aug. 2008.

[42] S. Wu and Y. Bar-Ness, "OFDM systems in the presence of phase noise: consequences and solutions," *IEEE Trans. Commun.*, vol. 52, no. 11, pp. 1988-1996, Nov. 2004.

[43] A. G. Armada, "Understanding the effects of phase noise in orthogonal frequency division multiplexing (OFDM)," *IEEE Trans. Broadcast.*, vol. 47, no. 2, pp. 153-159, Jun. 2001.

[44] A. G. Armada and M. Calvo, "Phase noise and sub-carrier spacing effects on the performance of an OFDM communication system," *IEEE Commun. Lett.*, vol. 2, no. 1, pp. 11-13, Jan. 1998.

[45] P. Robertson and S. Kaiser, "Analysis of the effects of phase noise in orthogonal frequency division multiplexing (OFDM) systems," in *Proc. Int. Conf. Commun.*, Seattle, WA, Jun. 1995, pp. 1652-1657.

[46] A. Demir, A. Mehrotra, and J. Roychowdhury, "Phase noise in oscillators: A unifying theory and numerical methods for characterization," *IEEE Trans. Circuit Syst. I*, vol. 47, pp. 655-674, May 2000.

[47] K. Nikitopoulos and A. Polydoros, "Compensation schemes for phase noise and residual frequency offset in OFDM systems," in *Proc. GLOBECOM*, San Antonio, TX, Nov. 2001, pp. 331-333.

[48] J. G. Proakis, *Digital Communications*, 4th ed. New York: McGraw Hill, 2001.

[49] R. Esposito and L. R. Wilson, "Statistical properties of two sine waves in gaussian noise," *IEEE Trans. Inform. Theory*, vol. IT-19, pp. 176-183, Mar. 1973.

[50] N. Y. Ermolova, "Capacity analysis of two-wave with diffuse power fading channels using a mixture of gamma distributions," *IEEE Commun. Lett.*, vol. 20, no. 11, pp. 2245-2248, Nov. 2016.

[51] S. H. Oh and K. H. Li, "BER performance of BPSK receivers over two-wave with diffuse power fading channels," *IEEE Trans. Wireless Commun.*, vol. 4, no. 4, pp. 1448-1454, Jul. 2015.

[52] A. K. Kohli and D. S. Kapoor, "Adaptive filtering techniques using cyclic prefix in OFDM systems for multipath fading channel prediction," *Circuits, Systems and Signal Process.*, vol. 35, no. 10, pp. 3595-3618, Oct. 2016.

[53] R. Garg and A. K. Kohli, "Parameter estimation and tracking of sinusoid using variable-step-size LMS algorithms," *Int. J. of Light and Elect. Optics.*, vol. 127, no. 22, pp. 10953-10960, Nov. 2016.

[54] A. Rai and A.K. Kohli, "Adaptive polynomial filtering using generalized variable-step-size least mean pth power (LMP) algorithm," *Circuits, Systems and Signal Process.*, vol. 33, no. 12, pp. 3931-3947, Dec. 2014.

[55] A. K. Kohli and D. K. Mehra, "Adaptive DFE multiuser receiver for CDMA systems using two-step LMS-type algorithm – An equalization approach," *Wireless Personal Commun.*, vol. 54, no. 3, pp. 543-558, Aug. 2010.

[56] A. Papoulis, *Probability Random Variables and Stochastic Processes*, 3rd ed. New York: McGraw Hill, 1991.

[57] G. J. Foschini and G. Vannucci, "Characterizing filtered light waves corrupted by phase noise," *IEEE Trans. Inform. Theory*, vol. 34, no. 6, pp. 1437-1448, Nov. 1988.

[58] D. D. Lin and T. J. Lim, "The variational inference approach to joint data detection and phase noise estimation in OFDM," *IEEE Trans. Signal Process.*, vol. 55, no. 5, pp. 1862-1874, May 2007.

[59] J. K. Sandhu and A. K. Kohli, "Impact of jammer noise on blind phase noise compensation in OFDM systems," *Intern. Journ. Latest Trends in Engg. and Tech.*, vol. 9, no. 4, pp. 76-82, Feb. 2018.

[60] A. K. Kohli, "Fading model for antenna array receiver for a ring-type cluster of scatterers," *Int. J. of Elec.*, vol. 98, no. 7, pp. 933-940, Jul. 2011.

[61] A. Bansal and A. K. Kohli, "Suppression of impulsive noise in OFDM system using imperfect channel state information," *Int. J. of Light and Elect. Optics*, vol. 127, no. 4, pp. 2111-2115, Feb. 2016.

[62] S. Sehrawat and A. K. Kohli, "Optimized mitigation of impulsive noise in OFDM system using CSI," *Int. J. of Light and Elect. Optics*, vol. 127, no. 20, pp. 9627-9634, Oct. 2016.

[63] A. K. Kohli and S. Garg, "High-rate STBC communication system using imperfect CSI under time-selective flat-fading environment," *Wireless Personal Commun*., vol. 99, no. 3, pp. 1231-1245, Apr. 2018.

LIST OF PUBLICATIONS

- A. K. Kohli and G. S. Lamba, "Impact of phase noise on single-tap equalization for fast-OFDM signals under generic linear fading channels," *Optik*, vol. 169, pp. 382-391, Published Online 2018. {SCI, IF = 1.191}